Deep-Sea Research Part II 152 (2018) 67–81

Contents lists available at ScienceDirect

Deep-Sea Research Part II

journal homepage: www.elsevier.com/locate/dsr2

Formation and transport of corrosive water in the Pacific Arctic region

Jessica N. Cross[a,*], Jeremy T. Mathis[b], Robert S. Pickart[c], Nicholas R. Bates[d,e]

[a] Pacific Marine Environmental Laboratory, National Oceanic and Atmospheric Administration, OERD-3, 7600 Sand Point Way NE, Seattle, WA 98115, USA
[b] NOAA Office of Ocean and Atmospheric Research, 1315 East West Hwy, Silver Spring, MD 20910-3282, USA
[c] Woods Hole Oceanographic Institution, 266 Woods Hole Rd., MS# 21, Woods Hole, MA 02543-1050, USA
[d] Bermuda Institute of Ocean Sciences, 17 Biological Station, Ferry Reach, St. George's GE 01, Bermuda
[e] University of Southampton, Department of Ocean and Earth Science, National Oceanography Centre, Southampton, UK

ARTICLE INFO

Keywords:
Ocean acidification
Pacific Arctic
Arctic Ocean
East Siberian Sea
Chukchi Sea
Beaufort Sea
Transport
Arctic Rivers
Sea Ice
Respiration
Upwelling
Biological vulnerability
Community resilience

ABSTRACT

Ocean acidification (OA), driven by rising anthropogenic carbon dioxide (CO_2), is rapidly advancing in the Pacific Arctic Region (PAR), producing conditions newly corrosive to biologically important carbonate minerals like aragonite. Naturally short linkages across the PAR food web mean that species-specific acidification stress can be rapidly transmitted across multiple trophic levels, resulting in widespread impacts. Therefore, it is critical to understand the formation, transport, and persistence of acidified conditions in the PAR in order to better understand and project potential impacts to this delicately balanced ecosystem. Here, we synthesize data from process studies across the PAR to show the formation of corrosive conditions in colder, denser winter-modified Pacific waters over shallow shelves, resulting from the combination of seasonal terrestrial and marine organic matter respiration with anthropogenic CO_2. When these waters are subsequently transported off the shelf, they acidify the Pacific halocline. We estimate that Barrow Canyon outflow delivers ~2.24 Tg C yr^{-1} to the Arctic Ocean through corrosive winter water transport. This synthesis also allows the combination of spatial data with temporal data to show the persistence of these conditions in halocline waters. For example, one study in this synthesis indicated that 0.5–1.7 Tg C yr^{-1} may be returned to the atmosphere via air-sea gas exchange of CO_2 during upwelling events along the Beaufort Sea shelf that bring Pacific halocline waters to the ocean surface. The loss of CO_2 during these events is more than sufficient to eliminate corrosive conditions in the upwelled Pacific halocline waters. However, corresponding moored and discrete data records indicate that potentially corrosive Pacific waters are present in the Beaufort shelfbreak jet during 80% of the year, indicating that the persistence of acidified waters in the Pacific halocline far outweighs any seasonal mitigation from upwelling. Across the datasets in this large-scale synthesis, we estimate that the persistent corrosivity of the Pacific halocline is a recent phenomenon that appeared between 1975 and 1985. Over that short time, these potentially corrosive waters originating over the continental shelves have been observed as far as the entrances to Amundsen Gulf and M'Clure Strait in the Canadian Arctic Archipelago. The formation and transport of corrosive waters on the Pacific Arctic shelves may have widespread impact on the Arctic biogeochemical system and food web reaching all the way to the North Atlantic.

1. Introduction

Ocean Acidification (OA) has a significant effect on marine biogeochemistry through the absorption of anthropogenic carbon dioxide (CO_2), both by lowering the pH of the surface ocean and the saturation states (Ω) of biologically important calcium carbonate ($CaCO_3$) minerals (e.g. Caldeira and Wickett, 2003; Sabine et al., 2004; Bates et al., 2014a). Seawater undersaturated with respect to $CaCO_3$ (i.e. $\Omega < 1$) is potentially corrosive for these minerals, and the emergence of corrosivity resulting from OA could have potentially negative consequences for calcifying organisms. Physiological impacts are dependent on organismal sensitivity and exposure to low pH and corrosive conditions.

Previous work has identified the Pacific Arctic Region (PAR; Fig. 1) as an OA hotspot (e.g. Fabry et al., 2009). Cooler water temperatures, ocean currents, and unique biogeochemistry precondition the regional carbon system to have a high sensitivity to anthropogenic CO_2 (Bates and Mathis, 2009a, 2009b). Without anthropogenic CO_2, these natural preconditioning processes do not produce seasonal or chronic undersaturations (Mathis et al., 2011a, 2011b). However, given this natural vulnerability, even small amounts of anthropogenic CO_2 can cause large

* Corresponding author.
E-mail addresses: Jessica.Cross@NOAA.gov (J.N. Cross), Jeremy.Mathis@NOAA.gov (J.T. Mathis), RPickart@WHOI.edu (R.S. Pickart), Nick.Bates@BIOS.edu (N.R. Bates).

https://doi.org/10.1016/j.dsr2.2018.05.020

Available online 22 June 2018
0967-0645/ Published by Elsevier Ltd.

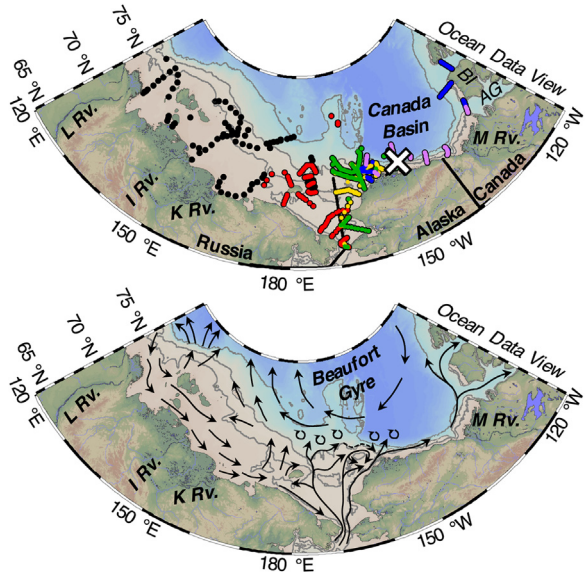

Fig. 1. Maps showing sampling locations (Upper Panel; see also Table 1), and mean circulation (Lower Panel) for this study. Colored dots indicate cruise occupation, including ISSS 2008 (black); RUSALCA 2009 (red); ICESCAPE 2010 (yellow); ICESCAPE 2011 (green); AON-OA 2011 (blue); and AON-OA 2012 (purple). The AON-OA mooring site at BS3 on the Beaufort Sea shelf break is indicated by a white X. Major geographical features are also noted, including the Lena, Indigirka, Kolyma and Mackenzie Rivers (L Rv., I Rv., K Rv., and M Rv., respectively); Banks Island (BI); Amundsen Gulf (AG); and the Canada Basin. The mean circulation pattern includes the Beaufort Gyre and the three primary pathways of flow through Bering Strait (Herald Valley, westernmost; Central Channel, centermost; and the Alaska Coastal Current (ACC), easternmost), after AMAP (1998); Woodgate et al. (2005b) and Pickart et al. (2016).

chemical changes and result in unnatural corrosivity that defines an OA event (Steinacher et al., 2009). In extremely corrosive hotspots, evidence of carbonate mineral dissolution has already been observed (Cross et al., 2013).

Future projections indicate that the duration, intensity, extent, and frequency of OA events in the PAR are likely to increase as anthropogenic CO_2 continues to build up (Steinacher et al., 2009; Mathis et al., 2015b). Rapid onset of persistently acidified conditions can have important consequences in highly sensitive systems like the PAR. The unprecedented pace of global anthropogenic acidification (Hönisch et al., 2012) can overwhelm natural physiological plasticity and population resilience, especially for larger species with lower reproductive rates (Hofmann et al., 2010; Boyd, 2011; Kelly and Hofmann, 2012). Global biogeochemical models have suggested that surface water corrosivity in the Chukchi and Beaufort Seas will pass outside the range of natural variability within the next 10–15 years (Mathis et al., 2015b), representing chronically acidified conditions. Initially, seasonal processes will mitigate these conditions during part of the year, but even these brief periods of respite will be overwhelmed by mid-century (Mathis et al., 2015b) as the system becomes acutely acidified. Given these expected changes, Punt et al. (2014) projected significant declines in populations of commercially important crab species in the Bering Sea, and a recent economic study estimated that current rates of OA already represent a significant risk to economic, cultural, and food securities in Alaskan communities (Mathis et al., 2015a).

As a result of these newly-emergent biogeochemical changes, ecosystem sensitivity, and rapid future progression of acidification, the PAR is commonly referred to as a bellwether for human-induced acidification (e.g. Fabry et al., 2009). Other rapid environmental changes like OA have already caused major shifts in Arctic marine ecosystems: for example, ocean warming, changes in atmospheric and oceanic circulation patterns, and sea-ice losses (Wassmann et al., 2011; Kulkarni et al., 2012; Grebmeier and Maslowski, 2014) have caused populations of temperate taxa to increase (Overland and Stabeno, 2004; Grebmeier et al., 2006) and primary production to rise (Leu et al., 2011; Tremblay et al., 2012; Arrigo and van Dijken, 2015). In particular, these changes are already visible in the diet and body condition of upper trophic marine mammals and birds (Moore and Stabeno, 2015). Because of these close linkages and tight biophysical coupling, many upper trophic species are sentinels for environmental changes (Moore et al., 2014; Moore and Gulland, 2014), and OA impacts could similarly propagate far up the food chain.

While it is clear that the ecosystem in the PAR is likely vulnerable to present and future OA conditions, the research community is just beginning to explore these vulnerabilities in detail. In part, these studies start with an assessment of the duration, intensity, and extent of current ecosystem exposure to corrosive conditions (e.g. Sigler et al., 2017). It is also critical to estimate the role of anthropogenic CO_2 in this corrosivity in order to attribute this exposure directly to OA. In some areas, corrosive conditions may be the natural result of regional biogeochemical cycles, and the ecosystem is likely correspondingly adapted (e.g. Hall-Spencer et al., 2008), while in others anthropogenic CO_2 pushes the system across key biogeochemical thresholds like the carbonate mineral saturation horizon (e.g. Feely et al., 2009). Understanding these components of OA exposure provides a baseline for future laboratory studies to assess species- and population-specific vulnerabilities (Sigler et al., 2017). Supporting these regional laboratory studies is especially important in the PAR, where many genetically distinct Arctic species and populations have yet to be assessed and may exhibit different responses than their sub-Arctic or tropical counterparts, similar to variability in response to temperature changes (e.g. Hollowed et al., 2013).

To initiate that effort, here we synthesize sub-regional process studies across four major recent programs in the East Siberian, Chukchi, and Beaufort Seas to provide this baseline assessment. We focus first on the unique mechanisms that contribute to natural carbon accumulation and corrosive water formation across the continental shelves of the PAR, exploring new insights into shelf-wide acidification mechanisms. We then combine these results with new moored data records that show the temporal persistence of acidified conditions during and after transport off the continental shelves. Lastly, we estimate the direct contribution of anthropogenic acidification to these corrosive conditions in order to assess the timing and rate of onset of chronic corrosivity. Overall, this synthesis highlights that anthropogenic acidification has drastically increased the duration, intensity, and extent of OA events in the PAR over the last several decades, and that present-day mitigation processes (e.g. upwelling) are relatively minor in comparison to the magnitude of acidification that has already occurred. We conclude by exploring the potential consequences of the rapid rate of onset of acidified conditions for PAR ecosystems over the last several decades, and how chronically acidified conditions may be impacting the present ecosystem structure.

2. Methods

2.1. Discrete data

The dataset used in this study was compiled from four Pacific-Arctic research programs that took place in summer and autumn between 2008 and 2012: the International Siberian Shelf Study (ISSS) in August/September 2008; the Russian-American Long-term Census of the Arctic (RUSALCA) in September 2009; the Impacts of Climate on Ecosystems and Chemistry of the Arctic Pacific Environment (ICESCAPE) in June/July 2010 and 2011; and the Arctic Observing Network (AON) Ocean Acidification Assessment (AON-OA) in October 2011 and 2012 (Fig. 1; Table 1). Together, these measurements span the Pacific inflow from

Table 1
PAR data compiled in this synthesis, including the International Siberian Shelf Study (ISSS) in the East Siberian Sea; the Russian-American Long-term Census of the Arctic (RUSALCA) in the Chukchi Sea; the Impacts of Climate on Ecosystems and Chemistry of the Arctic Pacific Environment (ICESCAPE) in the northeastern Chukchi Sea; and the Arctic Observing Network (AON) Ocean Acidification Assessment (AON-OA) in the Chukchi and Beaufort Seas. The number of samples in each dataset is indicated by *n*. For the mooring data, *n* is listed as well as the number of days spanned by the deployment.

Program	Dates	*n*
ISSS 2008	15 Aug–26 Sept	968
RUSALCA 2009	4 Sept–29 Sept	1200
ICESCAPE 2010	18 June–16 July	1167
ICESCAPE 2011	28 June–24 July	1652
AON-OA 2011	6 Oct–19 Oct	282
AON-OA 2012	11 Oct–21 Oct	1069
AON-OA Mooring	18 Oct 2012–15 Oct 2013	5807; 362 d

Bering Strait; mixing and modification over the Chukchi, East Siberian, and Beaufort Sea shelves; and transport into the Canada Basin and towards the Canadian Arctic Archipelago.

During each of the programs considered here, discrete samples were collected for dissolved inorganic carbon (DIC) and total alkalinity (TA), alongside additional variables such as temperature, salinity, nutrients, and dissolved oxygen concentration, much of which has been previously published (e.g. ISSS: Anderson et al., 2009; Semiletov et al., 2016; RUSALCA and ICESCAPE: Bates et al., 2013, Bates, 2015; AON-OA: Mathis et al., 2012; Evans et al., 2015). Each program used similar, highly precise sampling and analysis methods that conformed to community best practices (Dickson et al., 2007). During all programs, DIC and TA measurements were routinely calibrated using Certified Reference Material (CRM; supplied by A.G. Dickson, Scripps Institute of Oceanography). Each program reported statistical accuracy ≤ 2 µmol kg^{-1} (~0.1%). For this synthesis, extended carbon system variables (e.g. pH; partial pressure of carbon dioxide, pCO_2; aragonite saturation state, Ω_{Ar}) were calculated uniformly from the discrete temperature, salinity, phosphate, silicate, DIC and TA observations reported by each program using the CO_2calc software (Robbins et al., 2010). This application relies on specified carbonate dissociation constants. While there are many sets of equilibrium constants commonly used in the literature, we applied those from Millero et al. (2006). These were shown to provide the best comparison between calculated system variables and discrete samples for pCO_2 in the Arctic (Evans et al., 2015). Error in the calculation of Ω_{Ar} was estimated to be $\pm$ 0.10, after Dickson (2010) and Hydes et al. (2010).

2.2. Beaufort slope mooring

We also present new results here from the AON-OA moored time series, located at the BS3 mooring (Fig. 1). This time-series site was initiated during the Western Arctic Shelf-Basin Interactions program as part of a 7-mooring array spanning the Beaufort Sea shelfbreak and continental slope at 152°W. The original array helped to identify various processes associated with the Beaufort Sea shelfbreak current, including eddy activity (Spall et al., 2008a, 2008b) and upwelling events of Pacific halocline water that have visible impacts on primary production and CO_2 storage (Pickart et al., 2013; Mathis et al., 2012). Subsequent work has shown that the BS3 site alone, located in the center of the jet, can provide a holistic view of the boundary current behavior (Pickart et al., 2009). Accordingly, we assume that the data collected at BS3 are indicative of boundary current conditions in the Beaufort Sea. This in turn can help provide insights into the transport of carbon via winter-modified Pacific Water (Pacific Winter Water, PWW) at the edges of the East Siberian and Chukchi Sea shelves and the interaction with the Pacific halocline layer of the Arctic Ocean. Note that here we discuss the Pacific halocline as a single layer, given that it is difficult to differentiate variability in carbonate corrosivity between the upper and lower Pacific haloclines.

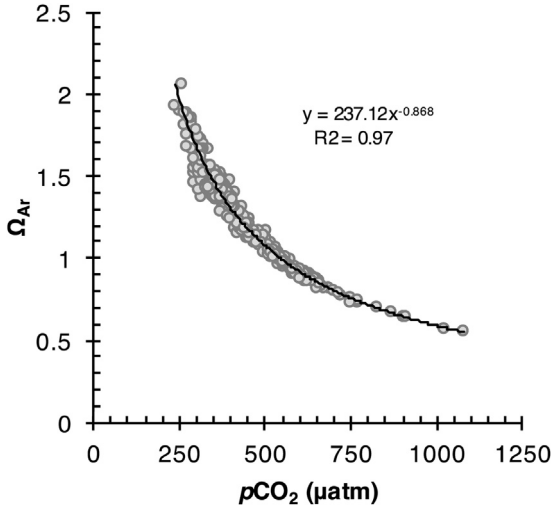

Fig. 2. Empirical relationship between pCO_2 and Ω_{Ar} derived from subsurface waters during HLY1203, including regression statistics.

In October of 2012, the AON-OA mooring was deployed in 147 m of water, instrumented with a 300 kHz ADCP, SBE39 MicroCat, and ULS-5 ice profiling sonar at 35 m; and a SAMI pCO_2 sensor and SBE39 MicroCat located at 127 m. Data were collected from 18 October 2012–15 October 2013. Discrete subsurface (> 35 m) DIC and TA data collected during the AON-OA cruise in 2012 were used to derive an empirical relationship between calculated pCO_2 and Ω_{Ar}, such that $\Omega_{Ar} = 237.12 \times pCO_2^{-0.868}$ ($r^2 = 0.97$; $n = 551$) (Fig. 2). According to this empirical fit, the data show that when pCO_2 values reached 545 $\pm$ 33 µatm (~6% error), Ω_{Ar} crossed the saturation horizon. Error was calculated as one standard deviation from the mean fit. It should be noted that the discrete data used to calculate this relationship were collected during October, and likely represent warmer temperatures than the annual mean. Given that the carbon system is extremely sensitive to temperature, it is important to note here that our empirical relationship is likely conservative—that is to say, during extremely cold periods, a lower pCO_2 value may correspond to the saturation horizon.

This conservative empirical relationship was applied to the pCO_2 time-series from the AON-OA mooring, creating a corresponding time-series for Ω_{Ar} according to the method of Mathis et al. (2013). This time-series shows the seasonal evolution of pCO_2 and Ω_{Ar} as PWW is transported off the shelf, enters the boundary current, and ventilates the Pacific halocline. The physical data from the AON-OA mooring were also used to create a record of wind-driven upwelling events via a graphical user interface (GUI; Supplemental Fig. 1). Upwelling events were defined using the alongcoast windspeed time-series from the Pt. Barrow, AK meteorological station, the along-isobath current velocity, and salinity averaged over the bottom 50 m of the water column. Upwelling is associated with an enhancement of the easterly winds, reversal of the shelfbreak jet (i.e. flow to the west), and an increase of near-bottom salinity (see Pickart et al., 2009 and Schulze and Pickart, 2012 for details). Although not considered here, other quantities such as satellite ice concentration and ice velocity from the mooring can be included in the GUI (e.g. Lin et al., 2016).

3. Results

The circulation and water masses of the PAR have been extensively reviewed in this volume (e.g. Bond et al., 2018; Citta et al., 2018; Logerwell et al., 2018; Moore et al., 2018; and Wang et al., 2018). To put the results of this synthesis study in context, we provide a schematic of the PAR circulation in the lower panel of Fig. 1, similar to those seen

in Logerwell et al., 2018 and Moore et al., 2018. Pacific Water (PW) preconditioned over the Bering Sea shelf enters the Chukchi Sea through three primary branches; the Alaska Coastal Current (ACC), driven by warmer, fresh water that flows along the Alaskan coast; a middle branch that flows through a topographic depression over the central Chukchi Shelf known as the Central Channel; and the western branch, which flows through Herald Canyon. During summer, most PW throughflow enters the Chukchi through the ACC and the Central Channel current branch (Gong and Pickart, 2015); during winter, transport over Hope Valley and through Herald Canyon comprises nearly 50% of the total throughflow (Woodgate et al., 2005b; Spall, 2007). Water also enters the Chukchi Sea from the East Siberian Sea shelf, which undergoes its own unique preconditioning processes. This water joins the westernmost branch of PW inflow. Over the northern Chukchi Sea shelf, flows are much slower and more complex, particularly near Hanna Shoal (e.g. Pickart et al., 2016).

These slow flows allow for extensive physical and biogeochemical preconditioning (see also Moore et al., 2018). Overall, the seasonal ice cycle partitions this inflow into two distinct water masses. Warming, ice melt and terrestrial freshwater runoff create a buoyant surface water layer that forms the Polar Mixed Layer (PML). Meanwhile, brine rejection and cooling occurring during ice formation produces a dense, saline water mass at the subsurface known Pacific Winter Water (PWW; Pickart et al., 2005). Shelf-basin interaction occurs as outflow through Barrow Canyon, the formation of eddies by instabilities near the shelf-break, and upwelling of deep waters. The variable Chukchi shelf-break jet (dotted line, lower panel Fig. 1) and the Beaufort shelf-break jet then carry this shelf-modified water towards the Canadian Archipelago.

As a 'first look' into the corrosivity of the PAR water masses, we present the relationship between temperature, salinity, and Ω_{Ar} across the data record for this synthesis in the upper panel of Fig. 3. A vector diagram showing the different water masses of the PAR by temperature and salinity is shown as an inset. In the deep waters of the Canada Basin, CO_2 concentrations are naturally very high, resulting in low Ω_{Ar} typical of deep waters across the world oceans. The warmer Atlantic halocline layer is supersaturated with respect to Ω_{Ar} (warm colors), while Ω_{Ar} undersaturations (cool colors) were observed in association with the low temperature extremes typical of PWW and the Pacific halocline layer of the Arctic Ocean basin. Here, we define the temperature / salinity range of PWW as $-1.8\,^{\circ}C < T < -1.4\,^{\circ}C$, $32.8 < S < 33.5$ (e.g. Woodgate et al., 2005a; Pickart et al., 2016). In this range, Ω_{Ar} values averaged 0.97. Note that Ω_{Ar} undersaturation was particularly pronounced during October of 2012 (average $\Omega_{Ar} = 0.78$; lower panel, Fig. 3, black grid lines). Surface water conditions across the synthesized data record showed Ω_{Ar} supersaturations in warmer PML waters. Some Ω_{Ar} undersaturations were present at the low-salinity extremes, associated both with river water and ice melt sources. (Note that these waters are typically corrosive endmembers; e.g. Yamamoto-Kawai et al., 2009; Mathis et al., 2011a, 2011b). These endmembers were easily identified in their respective datasets based on location (nearshore / offshore), depth (near surface), salinity, temperature, and TA.

Of all these water masses, transport of corrosive waters through the Pacific halocline layer has the potential to impact the greatest ecological area. Of the various water masses formed from the Pacific inflow, these Ω_{Ar} undersaturations are both the most persistent and the most widespread, as shown from the synthesized data above. These waters are regularly upwelled over the Beaufort Sea shelf and transported into the inlets of the Canadian Arctic Archipelago (Fig. 1; Pickart et al., 2013; Mathis et al., 2012; Shadwick et al., 2011). The Pacific halocline also penetrates deep into the Canada Basin, indicating the storage of a high volume of corrosive water that can be maintained for extensive periods of time in this stable water layer. In the following results sections, we explore the biogeochemical modification occurring over the shelves of the PAR that create these Ω_{Ar} undersaturations and the conditions that favor their persistence, ultimately resulting in Ω_{Ar} undersaturation in the Pacific halocline layer.

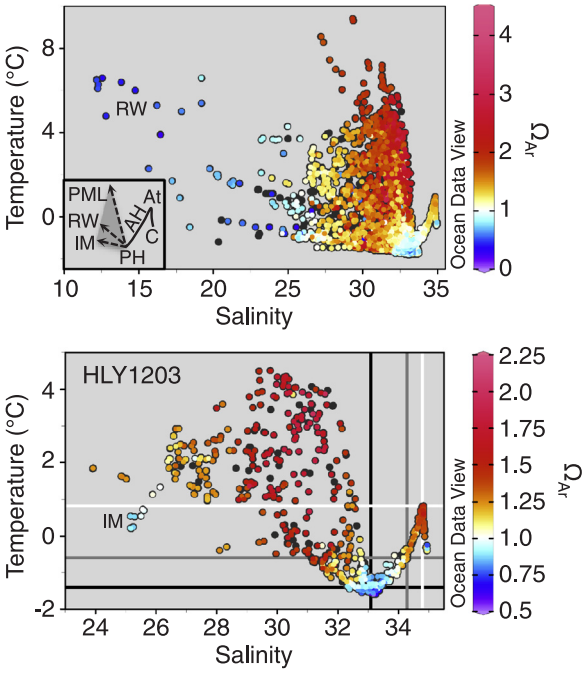

Fig. 3. Water masses, as defined by temperature, salinity, and aragonite saturation state (Ω_{Ar}). Ω_{Ar} supersaturations are indicated in warm colors, and Ω_{Ar} undersaturations are indicated in cool colors. The entire synthesis dataset is included in the upper panel, with an inset showing a water mass vector diagram identifying Polar Mixed Layer waters (PML); river waters (RW); ice melt (IM); Pacific Halocline waters (PH); Atlantic Halocline waters (AH); Atlantic Water (At); and Canada Basin Water (C). At the freshwater end, this vector diagram is more unconstrained, indicated by the dashed lines and darker grey shading. Note the presence of some Ω_{Ar} undersaturations in surface PML, RW, and IM. The bottom panel shows the data from the AON-OA 2012 cruise, including delineations for PH (black cross; S = 33.1; T = -1.4 °C), AH (grey cross; S = 34.3, T = -0.6 °C), and At (white cross; S = 34.8, T = 0.84 °C). This occupation shows clear undersaturations in Pacific waters. Ω_{Ar} undersaturations at the surface were associated with low-salinity ice melt near the ice edge.

3.1. Corrosivity in the Pacific inflow

During RUSALCA, supersaturations of Ω_{Ar} were observed over the southern Chukchi Shelf just north of Bering Strait. Identifying the mechanism contributing to these CO_2 supersaturations is extremely difficult given the lack of knowledge of carbon transport through Bering Strait. The Pacific inflow is known to be extremely nutrient-rich, supporting extensive seasonal phytoplankton phyotosynthesis (e.g. Codispoti et al., 2005) which could easily draw down CO_2 concentrations and favor Ω_{Ar} supersaturation. It is possible that mixing also acts to deplete CO_2 accumulation outside the production season. The warm, fresh, vertically mixed waters of the ACC are likely supersaturated due to extremely efficient sea-air CO_2 exchange, but it would be surprising for this process to extend to the central channel branch of the Bering Strait inflow. Given that very little carbon data are available north of St. Lawrence Island and south of Point Hope, discussion of these mechanisms are merely speculative.

Other work (Mathis et al., 2011a, 2011b; Cross et al., 2012) has hypothesized that intense biogeochemical preconditioning occurring over the southern Bering Sea shelf may contribute seasonally corrosive water generated in fall and winter to the Chukchi Shelf as it flows northwards. Ω_{Ar} undersaturations emerge in stratified bottom waters of the Bering Sea as early as June. These corrosive conditions intensify and expand geographically through fall (Mathis et al., 2013). During the Chukchi Sea occupations included in this synthesis, some of this

corrosive Pacific-origin winter-modified water should have been present over the shelf, but mixing and dilution during northward advection may have mitigated these Ω_{Ar} undersaturations. It is possible that sea-air CO_2 outgassing also contributed to the mitigation of these corrosive conditions, but it should be noted that limited CO_2 outgassing has only been observed over the Bering Sea Shelf during vertical overturning typical of the stormy autumn season (Cross et al., 2014).

3.2. Formation of corrosive conditions in the East Siberian Sea: the terrestrial pump

The mechanisms of biogeochemical modification over the East Siberian and Chukchi Sea shelves are better resolved than carbon transport through Bering Strait. Moving northward along the flow path of Pacific waters, the first Ω_{Ar} undersaturations encountered in this dataset were found through the RUSALCA program record, in the westernmost branch of the Bering Strait inflow at 68°N and 70°N. In particular, Ω_{Ar} undersaturations were observed in bottom waters on the western side of Herald Canyon and around Wrangel Island, which receives some source waters from the East Siberian Sea (Bates, 2015). It is possible that this corrosivity derives both from the respiration of locally produced and terrestrial organic matter. In order to investigate the formation and subsequent transport of this corrosivity, we will turn first to biogeochemical cycling that occurs in the East Siberian Sea.

The ISSS program and subsequent work have substantially added to inorganic carbon system observations in the Russian Arctic over the past decade (Anderson et al., 2010, 2013; Semiletov et al., 2016), especially in relation to the remineralization of terrestrial organic matter. The Lena, Indigirka, and Kolyma Rivers all drain into the Laptev and East Siberian Seas (see Fig. 1), comprising almost a third of the large river discharge in the Arctic Ocean basin. The chemistry of this terrestrial input is also unique: newly eroding soil and permafrost carbon from recent coastal erosion (e.g. Charkin et al., 2011; Semiletov et al., 2016) give the Lena River the highest flow-weighted average contribution of dissolved organic matter of any large Arctic river (762 µM; Cooper et al., 2008).

Much of this organic matter is respired near the coast; a sub-surface respiration signal is apparent near the Lena River outflow, indicated by depleted bottom water oxygen saturation levels and undersaturation with respect to Ω_{Ar} (see Fig. 4). In another study using these data, Semiletov et al. (2016) identified a terrestrial origin for this remineralized CO_2 using inorganic carbon isotopic data. The data shown here support that analysis; although pCO_2 values in the overlying surface plume were low (mean pCO_2 158 ± 35 µatm for S < 25) relative to atmospheric values (~386 µatm; Anderson et al., 2010; Tans and Keeling, 2016), oxygen saturation values were approximately 100%, indicating equilibration with the atmosphere. Oxygen saturation values typically exceed 100% during a bloom. The absence of a strong primary production signal confirms that autochthonous marine production is unlikely to be the source of this respired carbon in the bottom layer. Instead, the low surface pCO_2 values were likely created by dilution with river water.

In extremely shallow areas, mixing driven by winds, tides, and seasonal storm events can overturn the entire water column (e.g. Coachman, 1986; Kachel et al., 2002). The resulting ventilation can prevent CO_2 from building up in bottom waters (e.g. Cross et al., 2014) and rapidly erode corrosivity. However, stratification induced by river plumes can sometimes overcome and even exacerbate this CO_2 accumulation. A fine-scale analysis performed specifically for this synthesis showed that the overlying surface plume was also corrosive (mean Ω_{Ar} 0.54 ± 0.15 for S < 25). Freshwater discharge has been shown to have particularly poor buffering capacity (e.g. Cross et al., 2013; Evans et al., 2014), so even diluted surface CO_2 concentrations and lowered pCO_2 values can result in corrosivity due to diluted TA concentrations. Critically, this indicates that the plume was actively favoring influx of atmospheric CO_2 into already corrosive waters.

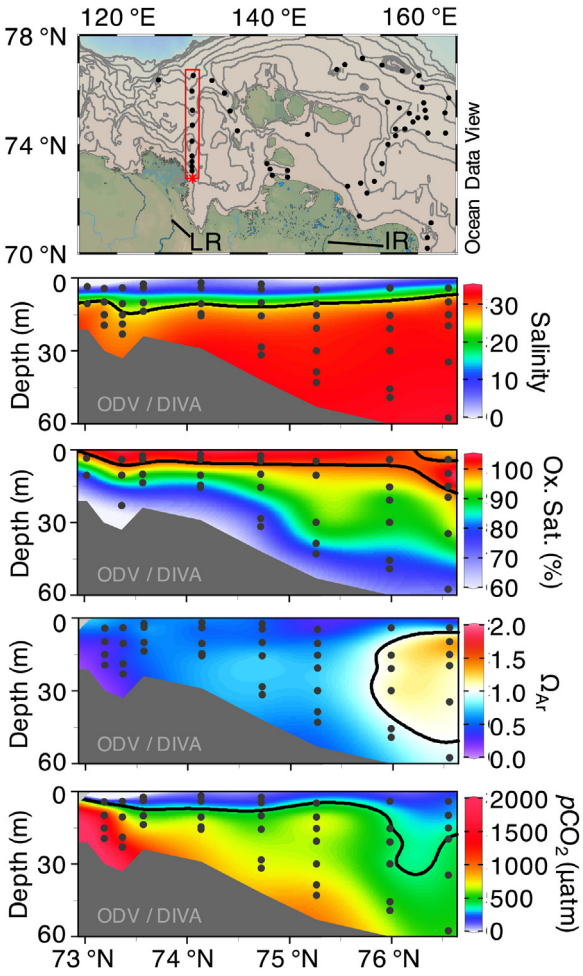

Fig. 4. Map of Laptev Sea section (red box, upper panel) and sectional plots showing salinity, oxygen saturation (%), Ω_{Ar}, pCO_2 (µatm). Note the Ω_{Ar} undersaturations (cool colors) penetrate all the way to the surface, where pCO_2 concentrations are concurrently low (cool colors).

Atmospheric CO_2 influxes to surface waters undersaturated with respect to Ω_{Ar} only occur across a small range of DIC and TA concentrations in the low-salinity spectrum due to thermodynamic constraints (Supplemental Fig. 2). However, while the plume remains concentrated, this unique chemistry can act to maintain high CO_2 concentrations in the underlying bottom layer and prevent CO_2 losses to the atmosphere, resulting in efficient transport of respired terrestrial CO_2 to at least the mid-shelf regions. This mechanism may be integral to the transport of corrosive waters to the Chukchi Sea. Over mid-shelf regions (i.e. > 40 m), this stratification eases and proximity to nutrient supply at the shelf break favors local primary production at the surface. This creates a secondary, mid-shelf insulation against CO_2 outgassing from bottom waters.

The overlap between these two insulating processes—river water discharge and primary production—was observed during both the ISSS and the RUSALCA programs. The influences of mid-shelf primary production are apparent at the northern end of the Lena River section shown in Fig. 4. Bates (2015) found moderate freshwater influences (e.g. mean S = 27.75 +/- 0.38 for 0–15 m) north and south of Wrangel Island in conjunction with low surface pCO_2 values relative to the atmosphere. In this case, low pCO_2 values occurred in conjunction with nutrient drawdown and oxygen supersaturation, indicating moderate local primary production. While these surface waters were not simultaneously corrosive, as near the Lena River plume, the low pCO_2 values did insulate the underlying corrosive bottom waters during

downstream transit into the Chukchi Sea. As a result, some corrosive inflow resulting from terrestrial organic matter respiration and the unique physical characteristics of river plumes are likely to influence at least the western branch of the Pacific inflow, and could have contributed to the corrosivity on the western side of Herald Canyon observed during the RUSALCA program.

However, this overlap is not ubiquitous. For example, Laptev Strait is extremely shallow and isolated from the mid-shelf by the Lyakhovksy Islands. Here, surface water CO_2 supersaturations were observed throughout the water column, indicating sea-air CO_2 outgassing (Supplemental Fig. 3). Surface water effluxes were also observed in the shallowest waters outside the Kolyma River, where the net influence of river water discharge had begun to weaken. At the edge of the river water plume, Anderson et al. (2010) found that CO_2 gas transfer rates were particularly high. However, just offshore, primary production again creates a surface layer drawdown of CO_2, insulating high CO_2 concentrations in bottom waters from potential outgassing to the atmosphere (Supplemental Fig. 3). At minimum, it is likely that ~60% of this respired terrestrial carbon is sequestered. Net primary production over the East Siberian Sea is estimated at ~13 Tg C yr^{-1} (Codispoti et al., 2013), based on non-carbon nutrient drawdown. A synthesis analysis of CO_2 fluxes in the region indicates 8 Tg C yr^{-1} ingasses from the atmosphere (Laruelle et al., 2014). To balance the annual primary production with the annual CO_2 influx requires a loss of ~ 5 Tg C yr^{-1} back to the atmosphere. Assuming that 100% of this balance comes from outgassing of respired terrestrial carbon in order to scale a minimum sequestration value, we estimate ~ 9 Tg C yr^{-1} (61.5%) of the total 14 Tg C yr^{-1} respired terrestrial carbon load estimated by Gustafsson et al. (2017) is retained in shelf waters for downstream transport.

3.3. Formation of corrosive water in the Chukchi Sea: the biological pump

Rates of primary production on the Chukchi Sea shelf are extremely rapid given the high nutrient supply from the Pacific inflow, exceeding 300 g C m^{-2} yr^{-1} (e.g. Hansell et al., 1993; Hill and Cota, 2005), and result in some of the lowest surface water carbon concentrations observed in the open ocean (Bates et al., 2011). Despite high grazing zooplankton biomass (e.g. Reigstad et al., 2008; Questel et al., 2013), the phytoplankton community is dominated by large species that sink quickly (Moran et al., 2005), leading to an uncoupling between primary production and grazing. This process can be especially rapid for ice-associated phytoplankton communities during sea-ice breakup, which favors aggregation and efficient export of the phytoplankton community as it is released from the ice substrate (Tremblay et al., 1989; Riebesell et al., 1991; Buesseler, 1998; Haeckey et al., 1998; Haeckey and Andersson, 1999; Fortier et al., 2002). Given the lack of retention of this carbon as upper trophic biomass, previous work has indicated that up to 75% of total primary production is exported from the mixed layer (Mathis et al., 2007), leading to efficient export of phytoplankton to colder, light-limited bottom waters and sediments where bacterial communities thrive. This carbon is subsequently remineralized, causing a seasonal buildup of CO_2 concentrations and corrosivity in bottom waters, similar to the respiration of terrestrial organic matter discussed above. In the Chukchi Sea, this seasonal corrosivity eventually becomes a characteristic of a new water mass, PWW.

During the ICESCAPE cruise in 2011, this water mass was already starting to form. Previous work has indicated that this area was the leading edge of winter water formation for the 2011 year (Lowry et al., 2015; Pickart et al., 2016), providing an ideal case to study how corrosivity builds up in PWW. Cool (< -1.6 °C) PWW was observed in conjunction with nutrient- and carbon-replete and low oxygen saturation conditions indicating respiration (Fig. 5). However, these conditions did not correlate precisely. Nitrate concentrations near-bottom varied more closely with density than with oxygen saturation or carbon parameters. Of the chemical products of respiration, retention and transport of nitrate is likely most efficient. Carbon and oxygen

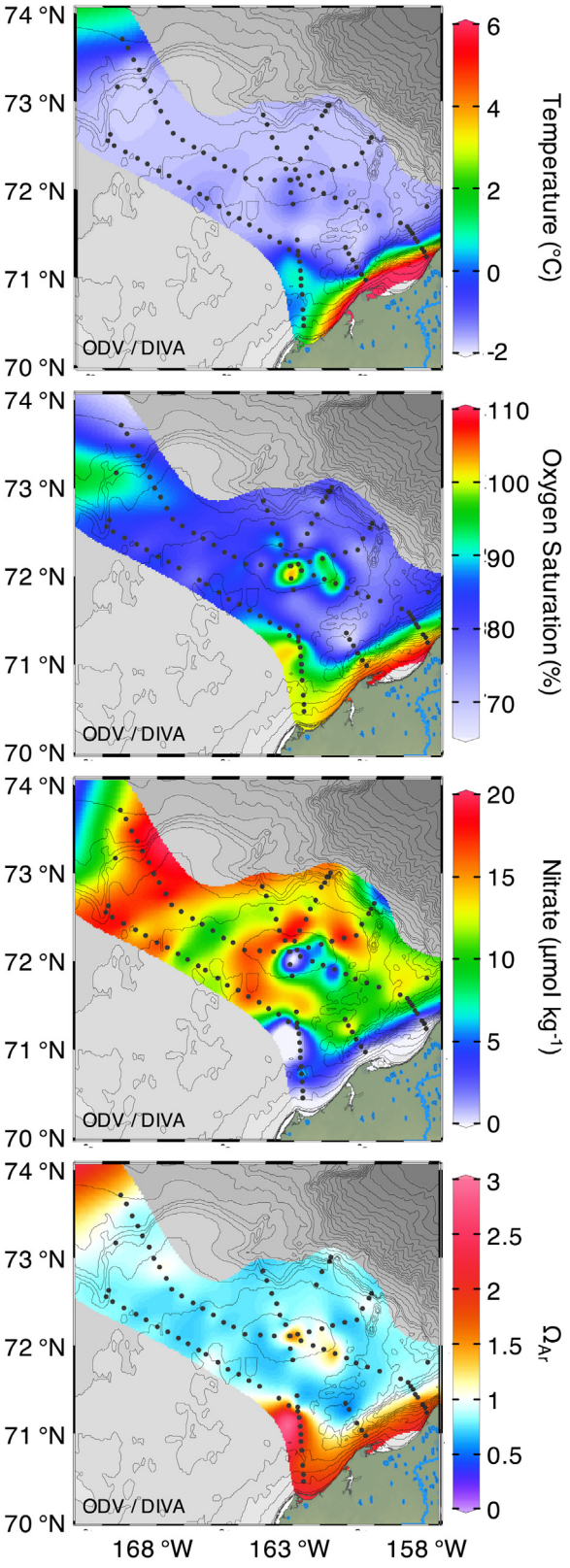

Fig. 5. Bottom water data for temperature (°C), oxygen saturation (%), nitrate (µmol kg^{-1}), and Ω_{Ar} in the eastern Chukchi Sea during ICESCAPE 2011. Note the area of Ω_{Ar} supersaturation, low nitrate values, and high oxygen saturation at the center of the shoal.

respiration signals are likely eroded through mixing and sea-air gas exchange, especially during fall storms, and even during ice-covered periods (Cross et al., 2013; Evans et al., 2015; Bates et al., 2014b). As a

result, carbon and oxygen signals correlate more tightly to each other than to nitrate or physical variables in shallow shelf regions. This thermodynamic decoupling of gases from the other winter-modification processes likely accounts for some of the spatial variability observed in these data at the leading edge of PWW formation.

Similar to the breakdown of stratification and sequestration of high CO_2 concentrations at the edges of river plumes discussed above, sequestration of gases may not be as efficient at the leading edge of winter water formation during spring. However, away from both the spatial and the temporal edges of this process, the biological pump does more efficiently transport carbon. Strong physical stratification and rapid export occurring at the peak and end of the spring bloom both favor sequestration of respiration products in the cooling bottom layer. For example, a nutrient study of the ICESCAPE 2010 and 2011 data by Lowry et al. (2015) found that the biological pump was much more active at the interface between winter water and warmer, shallower water with more light availability. This pump continues to operate beyond the June/July spring season and through the summer. During three monthly occupations of the Chukchi Sea shelf, Mathis and Questel (2013) observed a sharp increase in carbon accumulation between August and September, with the increase persisting through October as the bottom layer cooled.

The efficiency of carbon pumping into PWW can also vary interannually. For example, very limited corrosivity was observed during the 2010 ICESCAPE program, which took place during a similar time of year. However, during 2010, seasonal ice cover persisted for longer over the shelf, both delaying and limiting the formation of winter water (e.g. Gong and Pickart, 2015). During these years, weaker stratification does not provide optimum stability and nutrient supply for phytoplankton primary production. By contrast, during years with extensive open water, vigorous cooling and ice formation result in the formation of extensive amounts of winter water (e.g. Weingartner et al., 2005). Strong stratification at the surface also helps sequester respired CO_2 in subsurface layers.

3.4. Shelf-basin exchange of corrosive water

Transport of Pacific-origin water off the northern Chukchi Shelf occurs via several mechanisms and pathways. Each of the main branches of flow from Bering Strait through the Chukchi Sea ultimately drains into the basin (Fig. 1). Much of the water in the western branch forms an eastward-flowing shelfbreak jet along the northern edge of the Chukchi Sea after exiting Herald Canyon (Corlett and Pickart, 2017). However, most summer export occurs through Barrow Canyon, and some Canyon waters are derived from each branch. The Alaskan Coastal Current (ACC) flows through the eastern side of the canyon (Paquette and Bourke, 1974). This water is rapidly transported along the Alaskan coast, and spends the least amount of time over the Chukchi Sea shelf. The central channel branch feeds both sides of the canyon (Pickart et al., 2016). In contrast to the ACC pathway, some of the central channel branch is fed by waters from the slowest transport pathways across the Chukchi Shelf. Some of the western Bering Strait inflow branch is also diverted to the east just north of Herald Shoal (Pickart et al., 2010) and joins the central channel branch before draining into Barrow Canyon, also a very long transport pathway. These slow pathways favor focused deposition, provide ample time for biogeochemical modification during downstream transit, and are therefore likely preconditioned to exhibit corrosive signals.

The water that drains out of Barrow Canyon can take one of several routes. The water on the eastern side of the canyon—dominated by the ACC — tends to follow the isobaths as they bend to the east, forming the Beaufort shelfbreak jet (Nikolopoulos et al., 2009), downstream of the Herald Canyon shelfbreak jet. There is also turbulent outflow from the canyon in the form of eddies and filaments (Pickart and Stossmeister, 2008). Finally, some of the outflow veers to the west forming a current

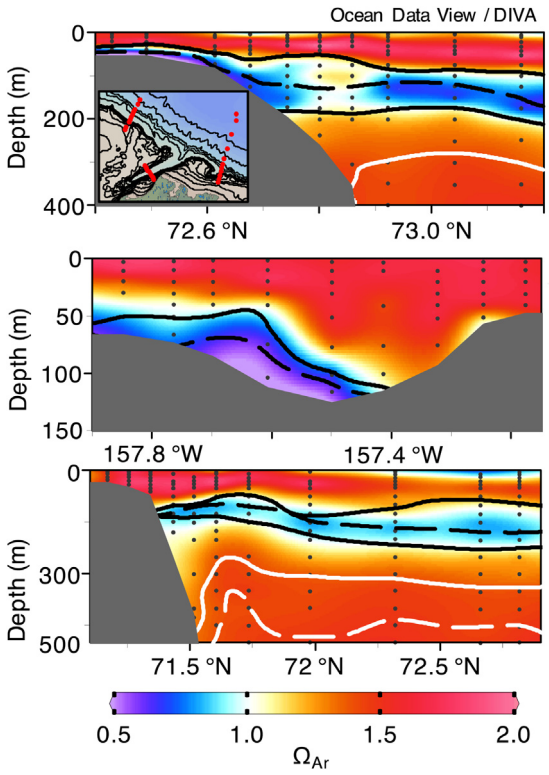

Fig. 6. Cross-shelf Ω_{Ar} sections near the Barrow Canyon outflow from the AON-OA 2012 cruise (inset), including northwest of Barrow Canyon (upper panel), across Barrow Canyon (middle panel), and southeast of Barrow Canyon (lower panel). Overlaid contours indicate water mass bounds, including PWW (T = -1 °C, solid black contours; S = 33.1, dashed black contour) and Atlantic Water (T = 0.5 °C, solid white contour; and S = 34.8, dashed white contour). The upper shows pulses of winter water flowing off the shelf; the middle panel shows low Ω_{Ar} stations on the west side of the canyon, flowing off of the Chukchi Shelf; and the lower panel shows Ω_{Ar} undersaturations in the Pacific halocline. Surface Ω_{Ar} undersaturations on the northern end of this line were associated with ice melt.

over the Chukchi continental slope. This recently discovered feature has been named the Chukchi Slope Current, which accounts for up to half of the outflowing transport from Barrow Canyon (Corlett and Pickart, 2017). Notably, both the Chukchi and Beaufort shelfbreak jets as well as the Chukchi Slope Current are known to be baroclinically unstable (Pickart et al., 2005; Spall et al., 2008a, 2008b; Corlett and Pickart, 2017), which promotes shelf-basin exchange. Eddies of Pacific-origin are commonly found off the shelfbreak, the most common of which are cold-core anti-cyclones. These features are believed to be a significant source of carbon and nutrient transport from the northern Chukchi Sea (Mathis et al., 2007).

Several sections in the vicinity of Barrow Canyon are shown in Fig. 6. Corrosive conditions associated with PWW are found in each of the transects. The section to the west of Barrow Canyon (upper panel of Fig. 6) shows two extrema of corrosive PWW, one within the eastward-flowing shelfbreak jet closer to shore, influenced by outflow from Herald Canyon and chaotic shelf-basin exchange off the northern Chukchi shelf, and the other within the westward-flowing Chukchi slope current situated farther offshore. The section through the center of Barrow Canyon (center panel of Fig. 6) shows the Ω_{Ar} - undersaturated winter water banked on the western flank of the canyon. Some of this dense water can transpose to the eastern flank and exit the canyon in the Beaufort shelfbreak jet (Pickart et al., 2005), while some of it exits to the west in the Chukchi slope current further offshore, likely influencing the signal shown in the upper panel. The eastern side

of the canyon contains warmer and fresher Alaska Coastal Water which is largely supersaturated with respect to Ω_{Ar}. This is likely because the fast-moving current promotes strong mixing which would lead to extremely efficient sea-air CO_2 equilibration and higher Ω_{Ar}, as discussed earlier.

As the water from both sides of the canyon exits into the Beaufort shelfbreak jet, the surface ACC current insulates the denser water transposed from the western side of the canyon from sea-air exchange. The section to the east of Barrow Canyon (lower panel of Fig. 6) crosses the Beaufort shelfbreak jet. This current carries the corrosive signature of PWW eastward towards the Canadian Arctic Archipelago. Additional biogeochemical conditioning by respiration is limited, as nutrient availability restrains primary production over this narrow shelf. While previous work has considered permafrost degradation as a potential source of labile organic matter to this region, recent work indicates that respiration of permafrost carbon at the shelfbreak is limited (Hilton et al., 2015). Note that this transect extends far into the interior, demonstrating that corrosive PWW ventilates the halocline throughout the Canada Basin.

Another mechanism of shelf-basin exchange along the Beaufort slope is wind-driven upwelling. Easterly winds drive offshore Ekman transport of surface waters, while halocline waters are drawn up onto the shelf (Pickart et al., 2009). Upwelling events are common throughout the year and occur in all ice conditions as long as pack-ice is mobile (Schulze and Pickart, 2012). Recently, new data from the AON-OA program showed that this can lead to rapid outgassing of CO_2 stored in the halocline by earlier shelf-basin exchange (Mathis et al., 2012). Initially, these upwelling events flush the entire shelf with corrosive halocline waters (Fig. 7), but sea-air CO_2 equilibration diminishes this corrosivity over time, partially mitigating the accumulation of carbon and Ω_{Ar} undersaturations in the Pacific halocline. Upwelling has also been observed along the Chukchi shelfbreak (Llinás et al., 2009; Spall et al., 2014), though the frequency and commonality of these events are unknown.

3.5. Downstream transport of corrosive Pacific waters

The balance between the carbon pumped into the halocline of the Canada Basin from the East Siberian, Chukchi, and Beaufort Sea shelves and the upwelling occurring along these shelfbreaks ultimately determines the net amount of corrosive water fluxed offshore. Using 6 years of mooring data at the mouth of Barrow Canyon, Itoh et al. (2012) determined that the annual mean northward transport of PWW was 0.23 Sv, where they defined winter water as generally colder than −1.5 °C and saltier than 32.0 (which accounts for both regular winter water and hypersaline winter water). Based on an average DIC concentration of 2200 μmol kg^{-1} in Ω_{Ar} undersaturated PWW across this density range (25.8–27.5 kg m^{-3}), this results in a delivery of 4.94–5.27 Tg C to the western Arctic Ocean in one year. The new moored observations at the AON-OA time-series site synthesized with the AON-OA shipboard data here provide an opportunity to consider how much of this carbon may be lost to sea-air CO_2 gas exchange during upwelling events after departing the shelf, and provide some insights into how efficiently this system can maintain Ω_{Ar} undersaturations over time once PWW exits the shelf.

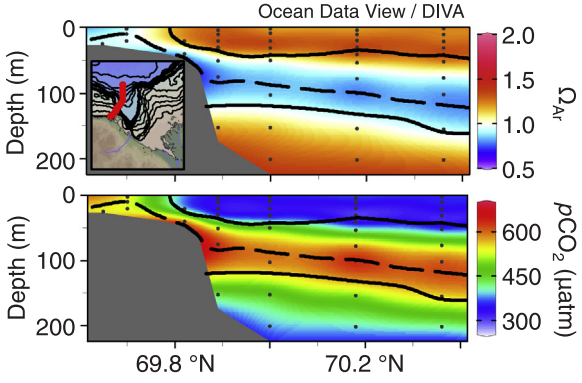

Fig. 7. Cross-shelf sections showing Ω_{Ar} and pCO_2 (μatm) offshore of the Mackenzie River (inset) during the 2011 AON-OA cruise. Note the low Ω_{Ar} and high pCO_2 at the neashore, indicative of an upwelling event.

Fig. 8 shows the calculated Ω_{Ar} at the AON-OA time-series site. These data were collected at 127 m depth, in the center of the corrosive Pacific halocline layer (Nikolopoulos et al., 2009; see also Fig. 6). Overall, temperature and Ω_{Ar} vary closely with each other, with the cold PWW (< −0.1 °C) almost uniformly corrosive, consistent with the water mass diagram shown in Fig. 2. Corrosive conditions were found over the shelf for 290 days, or 80% of the year-long deployment. Ω_{Ar} values were below 0.75 (severely corrosive) for 110 days, or 30% of the year-long deployment. Periodic Ω_{Ar} supersaturations were found dominantly between October and March of 2012. After April, Ω_{Ar} values were consistently undersaturated, and gradually decreased through the following September. Ω_{Ar} supersaturations always coincided with the presence of warmer waters and frequently with indicators of upwelling events, even during complete ice cover. This is consistent with the results of Schulze and Pickart (2012) who found that almost 90% of strong easterly wind events, regardless of season and ice cover, resulted in upwelling.

The wind-driven upwelling events in Fig. 8 were identified using along-coast wind speed (from the Pt. Barrow weather station), along-slope velocity, and salinity in the bottom layer (see Section 2.2). A typical event begins when easterly winds exceed 4 m s^{-1}, followed roughly 8 h later by a reversal of the shelfbreak jet. This current usually flows eastward towards the Canadian Arctic Archipelago, but easterly winds readily reverse its direction. Upwelling commences roughly 10 h after the flow reverses, bringing saltier water past the mooring site. The period of upwelling is identified using the GUI when the near-bottom salinity exceeds the monthly mean value (see Schulze and Pickart, 2012 for details). As seen in Fig. 8, the presence of Ω_{Ar} supersaturations correlates well with upwelling activity during the winter months (November–March). Most of these events brought Atlantic Water past the mooring site. By contrast, the upwelling events during the warm months did not generally correspond to an increase in saturation. This is because many of those events brought denser PWW past the mooring. This seasonal variation in upwelling (Atlantic Water events in winter, Pacific Water events in summer) is typical of the Beaufort Slope (Lin et al., 2016).

Importantly, during both types of upwelling, PWW is typically advected onto the shelf (Schulze and Pickart, 2012), where it can have substantial impacts on the carbon system. Fig. 7 shows an example of a Pacific Water event that flooded the entire shelf with corrosive waters. Mathis et al. (2012) showed that the 10-day open-water upwelling event captured in Fig. 7 led to substantial CO_2 outgassing (0.18–0.54 Tg C yr^{-1}), and estimated that four such events could completely balance the net uptake of CO_2 that occurs in the Beaufort Sea during primary production (2–3 Tg C yr^{-1}). In our dataset, three upwelling events of sufficient duration (> 10 d) occurred during open water periods (July–September; Table 2), alongside four smaller events. If environmental conditions at the surface were similar to those observed by Mathis et al. (2012), we estimate a total CO_2 flux of 0.5–1.7 Tg C across the total 33 days of wind-forced upwelling conditions (Table 2).

Some additional loss of carbon to the atmosphere is likely during the winter months. A number of recent studies have begun to quantify CO_2 fluxes through sea ice. Amid inconsistent results and varying methods for field testing of flux through sea ice, the community has broadly adopted a proxy that linearly reduces gas transfer velocity relative to sea-ice concentration such that: Flux(ice) = Flux × (1 – sea-ice concentration). This parameterization has recently been confirmed in the Southern Ocean marginal ice zone (Butterworth and Miller, 2016). For ice concentrations at 90–95%, as would be typical of the Beaufort Sea

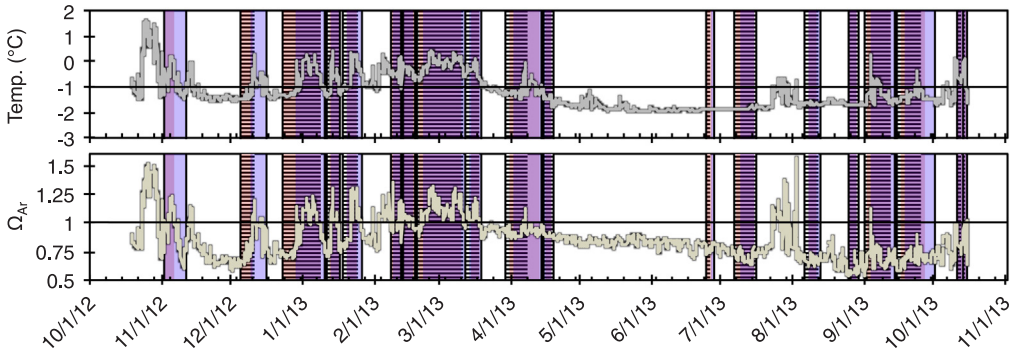

Fig. 8. Time-series record of temperature (°C) and Ω_{Ar} from the AON-OA Mooring site (127 m) during 2012–2013 deployment. Raw pCO_2 data were converted using the empirical relationship given in Fig. 2. Color shading indicates upwelling-favorable conditions according to salinity (blue), velocity (red), and wind (textured dots). Co-occurrence of these features is indicated in shaded purple.

Table 2
Number of days of upwelling-favorable conditions indicated by sustained negative anomalies in zonal easterly 10 m windspeed; negative anomalies in depth-integrated along-isobath zonal current velocity; positive anomalies in depth-averaged salinity across 50–150 m; positive anomalies in Ω_{Ar}; and sustained periods of Ω_{Ar} supersaturation. All anomalies are calculated relative to the annual mean value for the variable. Dark colors indicate statistically long periods of upwelling favorable conditions relative to the mean duration. Lighter colors indicate statistically insignificant but above-average event duration. Undetectable and negative anomalies are not shown (blank values).

Start Date	Wind	Velocity	Salinity	Ω_{Ar}	$\Omega_{Ar} > 1$
	Days	*Days*	*Days*	*Days*	*Days*
2-Nov		4.68	9.06	5.88	3.38
5-Dec	6.25	4.81	6.94	4	3.56
23-Dec	**16.56**	**16**	**12.43**	9.38	7.38
11-Jan	5.8	3.3	3.25	2.19	2.19
18-Jan	2.75	4.44	6.06	6.13	5.63
8-Feb	4.44	3.94	3.44	2	1.68
13-Feb	4.75	4.44	4.31	7.81	5.19
19-Feb	**21.75**	**19.38**	**19.31**	**26.81**	**26.75**
12-Mar	6.13	3.38	5.81	6.63	
29-Mar	**10**	**13.5**	**12.5**	**10.19**	1.31
15-Apr	3.81	2.25	2.69		
24-Jun	2.31	2.75	1.44		
6-Jul	**10.06**	8.69	6.31		
6-Aug	6.75	4.69	6.5		
25-Aug	3.38	2.56	2.69		
1-Sep	**11.13**	9.5	**10.5**	0.63	0.44
15-Sep	**10.38**	**11.31**	**13.38**		
11-Oct	1.69	2	1.94	1.56	
AVERAGE	7.53 ± 5.19	6.76 ± 5.02	7.14 ± 4.71	7.03 ± 6.70	4.14 ± 2.02

during the winter months, fluxes would be reduced to 0.5–1% of their open water value. This would result in an additional efflux of 0.01–0.02 Tg C yr^{-1} to the atmosphere.

This loss of carbon due to upwelling events (maximum 1.72 Tg C yr^{-1}) balances 9.45–32.26% of carbon transport from winter water. Averaged over the depth of the boundary current and along the area of the entire Beaufort Sea shelf (9×10^{12} m^3), this upwelling signal could reduce DIC concentrations in winter water by 184 μmol kg^{-1} on average, which would be more than sufficient to alleviate Ω_{Ar} undersaturations in upwelled waters in this case. This scales well with the data record showing that corrosive conditions are present in the Beaufort Sea boundary current ~80% of the year. It is likely that this corrosivity is persistent except in the presence of direct, episodic influences.

4. Discussion

4.1. Ocean acidification in the Pacific Arctic Region

As a global system, the oceans have absorbed approximately 28% of the CO_2 emissions released into the atmosphere by human activity in the last century. Of this anthropogenic carbon, nearly 40% resides in the Pacific Ocean alone (Sabine et al., 2004). Based on previous global and local studies (Sabine et al., 2004; Cross et al., 2013; Le Quéré et al., 2015), a conservative estimate suggests that the North Pacific and Arctic Ocean contain approximately 65 μmol kg^{-1} anthropogenic CO_2. Accordingly, the estimated pre-industrial condition and the present extent of corrosive waters based on our data synthesis are shown in Fig. 9. Near-bottom values are displayed over the continental shelf, while the Pacific halocline layer is displayed in the basin and across the shelfbreak. For most areas of the continental shelf, especially in the Chukchi and Beaufort seas, Ω_{Ar} undersaturations have appeared directly as a result of anthropogenic CO_2, although some areas close to the saturation horizon ($\Omega_{Ar} = 1$) are evident, especially west of Wrangel Island. Surprisingly, the pre-industrial environment does reflect corrosive conditions downstream of the Lena River outflow. By our calculations, more than double the amount of CO_2 would need to be removed in order to induce Ω_{Ar} supersaturations in this area. While we have considered our 65 μmol kg^{-1} estimate of anthropogenic CO_2 conservative, it is likely that Ω_{Ar} undersaturations are a natural phenomenon in this area and the local ecosystem is likely adapted to these conditions.

The discrete data from 2008 to 2012 show the emergence of corrosive waters across the area over time. The intensity and extent of natural Ω_{Ar} undersaturations observed near the Lena River outflow worsened substantially into the present day ($\Omega_{Ar} < 0.5$), while new, unnatural Ω_{Ar} undersaturations have emerged in all three Arctic shelf seas. These patterns are particularly pronounced in areas known to be hotspots for bacterial respiration, where currents are weak and respiration products can build up more efficiently over time. Notably, areas that are extremely shallow (e.g. Hanna and Herald Shoals, Wrangel and Banks Island coasts) and the fast-moving Alaska Coastal Current remain supersaturated with respect to Ω_{Ar}. These areas are particularly susceptible to consistent vertical overturning, which likely favors air-sea exchange of CO_2 and does not permit sub-surface buildup of CO_2 and Ω_{Ar} corrosivity.

One of the most notable aspects of Fig. 9 is the spreading of corrosive conditions into the Pacific layer of the halocline since pre-industrial times. This implies that widespread acidification of the halocline is a recent phenomenon driven by anthropogenic CO_2. An anthropogenic CO_2 absorption rate of 0.86 + /- 0.12 μmol kg^{-1} yr^{-1} has been observed in the sub-Arctic North Pacific (Watanabe et al., 2011). By linearly extrapolating this rate backwards from the present condition, we estimate that corrosive conditions first appeared in the Pacific halocline between 1975 and 1985, where DIC concentrations were only 24–32 μmol kg^{-1} lower than at present. This coincides closely with estimates that the Bering Sea shelf waters to the south were completely saturated with 45 μmol kg^{-1} anthropogenic CO_2 in 1983 (Chen, 1993), and with recent observations of the buildup of corrosive halocline waters in the northern Chukchi Sea and adjacent Canada Basin (Qi et al., 2016). Importantly, this indicates that the East Siberian Sea has contributed naturally corrosive water to the Pacific halocline through transpolar drift, eddy formation, and other forms of shelf-basin

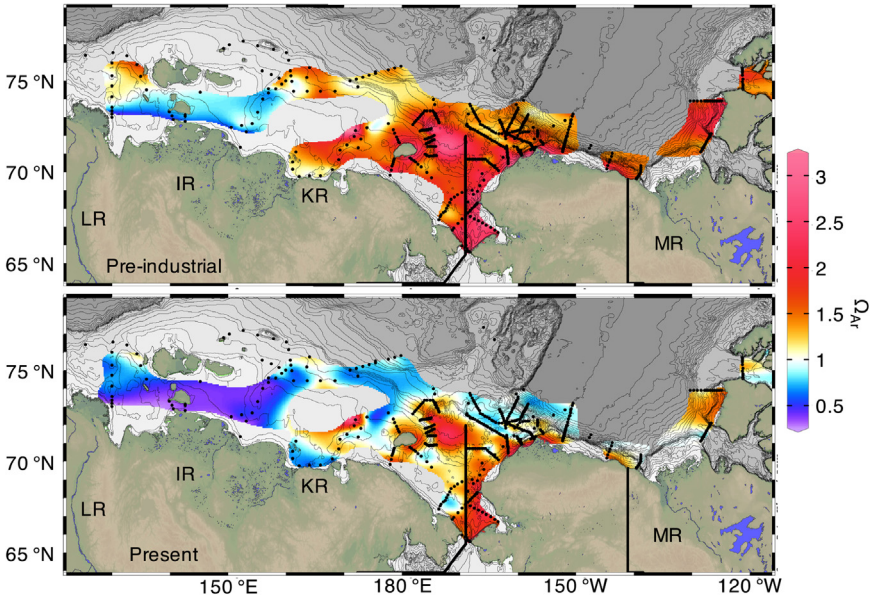

Fig. 9. Aragonite saturation states (Ω_{Ar}) in PWW (28.1 ≤ S ≤ 33.75 and T ≤ -0.5 °C) in the Pacific Arctic Region (PAR) in the pre-industrial setting (upper panel) and present-day (lower panel). Pre-industrial estimates were made by subtracting 65 μmol kg^{-1} anthropogenic CO_2 from the present day DIC values, and recalculating Ω_{Ar}. Strong Ω_{Ar} supersaturations are found in the well-mixed, fast moving currents in the Chukchi Sea along the Alaskan coast and central channel, but slowing currents over the northern Chukchi Shelf allow for the accumulation of respiration products and lower Ω_{Ar}. These waters then exchange across the slope, contributing to Ω_{Ar} undersaturations in the Pacific halocline layer in the Canada Basin. These waters extend through the entrances to Amundsen Gulf and M'Clure Strait, showing the extensive reach of the physical and biogeochemical modification occurring over the northern Chukchi and East Siberian shelves.

exchange over time without inducing widespread Ω_{Ar} undersaturation across the halocline. This natural phenomenon was not enough to induce widespread corrosivity in the absence of anthropogenic CO_2.

Our data indicate that Ω_{Ar} undersaturations extend all the way into the Canadian Arctic Archipelago, including the entrances to Amundsen Gulf and M'Clure Strait. While this synthesis does not extend further, other researchers have traced this Pacific-origin carbon through the entire length of the Archipelago and into the North Atlantic (Shadwick et al., 2011; Yamamoto-Kawai et al., 2013). Just as expanding Ω_{Ar} undersaturations have been observed in the Pacific halocline, it is likely that corrosive conditions will also begin to progress through the Canadian Archipelago. Pacific source waters are already at or near Ω_{Ar} undersaturation in Baffin Bay and the Labrador Sea (Azetsu-Scott et al., 2010), and compounding carbon accumulation factors could have important implications for the highly productive ecosystems of the Canadian Arctic and the multi-billion dollar commercial fish and shellfish industries on the Atlantic side.

4.2. Potential ecosystem vulnerabilities and resilience

As indicated at the start of this paper, mapping corrosivity over the PAR as we have here is critical to understanding potential ecosystem impacts. OA is projected to have negative physiological effects on many species (Kroeker et al., 2010), including reduced shell or skeletal strength, growth, and integrity to slower growth rates, competitive disadvantage, and reduced survival, especially for some early life history stages with limited coping and internal regulatory capacities (see broad reviews of variable organismal response to OA by Fabry et al., 2008; Doney et al., 2009; Kroeker et al., 2010; Ferrari et al., 2011; Joint et al., 2011; Andersson and Gledhill, 2013). The risk of negative impacts is dependent on the duration, intensity, and extent of acidified conditions, population and life stage exposure to those conditions, and species-specific vulnerability and resilience to these hazards. Here, we have shown the persistent duration and widespread spatial extent of acidified conditions. The newly acidified waters in the eastern East Siberian Sea, the northern Chukchi Sea, the Beaufort Sea shelf break and the inlets of Amundsen Gulf and M'Clure Strait (Fig. 9) certainly represent a significant change in environmental conditions that constitutes new exposure to acidified conditions.

While continuing research will be required to show the species- and population-specific vulnerability to the present and future acidified conditions, bedrock species in the Alaskan food web have already shown vulnerabilities to OA in the laboratory setting. For example, zooplankton like copepods and euphausiids that support large swaths of upper trophic predators from seabirds to whales have shown poor internal ionoregulatory capacity. In response to OA, zooplankton species have displayed reduced hatch rates, delayed embryonic development, and increased post-larval energy demands that could impact overwintering survival and their energy quality as prey (euphausiids: generally, McBride et al., 2014; *Euphausia superba*, Kawaguchi et al., 2013; *Euphasia pacifica*, Cooper et al., 2016 and McLaskey et al., 2016; copepods: *Acartia erythera* and *Acartia tonsa*, Cripps et al., 2014; *Pseudocalanus acuspes*, Thor and Oliva, 2015). Seals, walrus, and marine birds (e.g. *Erignathus barbatus, Odobenus rosmarus*, *Somateria fischeri*) may be impacted by the inherent vulnerability of calcifying benthic invertebrates and bivalves in their prey base (generally, Kurihara, 2008; *Mytilus edulis, Crassostrea gigas*, Gazeau et al., 2007, 2013; *Mercenaria mercenaria* and *Argopecten irradians*, Talmage and Gobler, 2010; *Macoma calcarea* and *Mytilus galloprovincialis*, Vihtakari et al., 2016; *Macoma calcarea, Astarte montagui,* and *Astarte borealis*, Goethel et al., 2017). Early life stages of important commercial species have also displayed laboratory vulnerability to acidified conditions, like larval Arctic and Atlantic cod (Atlantic cod: *Gadus morhua*, Frommel et al., 2012, Stiasny et al., 2016, and Dahlke et al., 2016; Arctic cod: *Boreogadus saida*, Kunz et al., 2016) and juvenile (Long et al., 2013b) and adult (Long et al., 2013a) red king and tanner crab (*Parlithodes camtschaticus*, *Chinoecetes baridi*) that could ultimately reduce recruitment to the fished population (Punt et al., 2014).

As shown in Fig. 9, OA exposure is particularly pronounced for two important macroecological environments in the Chukchi Sea: the seasonal ice zone, and the advective pathways between the Pacific and the Arctic Oceans (Carmack and Wassman, 2006; Bluhm et al., 2014; Wassman et al., 2015; Moore et al., 2018). Given the short linkages that characterize the food web in the PAR, OA impacts on important prey species like zooplankton and bivalves can quickly cause a reduction in food supply for corresponding predators. In acidification hotspots like Hanna Shoal in the northern Chukchi Sea (see Figs. 5 and 9), several species of seabirds (especially crested auklets; *Aethia cristatella*, Kuletz et al., 2015) and walrus (*Odobenus rosmarus*, Jay et al., 2012 and Kuletz et al., 2015) are found in very high densities during summer and fall. Additionally, the four core-use habitat areas for bowhead whales north of Bering Strait (*Balaena mysticetus,* Citta et al., 2015 and Okkonen et al., 2018) are all located in seasonally acidified areas identified here. Advected zooplankton that join the slow transport pathways through

the Central Channel are likely to experience extended exposure to acidified conditions. Even for those organisms that end up on the shelf break of the Chukchi and Beaufort seas through the non-corrosive transport pathways like the Alaska Coastal Current, diurnal vertical migration (*Eurytemora affinis, Acartia bifilosa*, Almén et al., 2014; *Euphausia pacifica,* Cooper et al., 2016) and copepod diapause (*Calanus* spp., Mayor et al., 2015) expose these organisms to the persistently acidified Pacific halocline layer.

Linking these documented species vulnerabilities to the exposure to severe, sustained, and widespread acidified conditions in the Pacific Arctic suggests that important changes may be in store for the Chukchi ecosystem. However, it is critical to note that at the present time, there is limited evidence that exposure to OA has caused serious population declines or change in the Pacific Arctic ecosystem. In part, this may suggest stronger natural resilience than short-term (e.g. single-generation) laboratory studies indicate. Phenotypic and species diversity can represent adaptive capacity in some cases: when one phenotype or species is selectively impacted by OA, the overall population can recover as a better-adapted phenotype or species gains a competitive advantage. While adaptive capacity can be difficult to study in the laboratory, longer-term laboratory studies show that high-latitude copepod populations have demonstrated adaptive capacity to acidified conditions within just two generations of selection (*Pseudocalanus acuspes*, Thor and Dupont, 2015; De Wit et al., 2015). Relative to the time of emergence of anthropogenically-mediated corrosivity over the last several decades, this adaptation is far more rapid (~180 d), indicating that the current pace of acidification has not overwhelmed this natural plasticity. Additionally, other forms of ongoing Arctic environmental change may actually alleviate OA stress. Sufficient food supplies have been shown to confer resistance to acidification (e.g. corals, molluscs, crustaceans, and echinoderms, Ramajo et al., 2016). If phytoplankton production increases in the Arctic in response to warming temperatures and ice losses (e.g. Arrigo and van Dijken, 2015; Hill et al., 2018) this may be an emerging form of resilience.

However, these small-scale forms of resilience are finite. Metabolic upregulation from increased food consumption can only be sustained up to a certain point (Ramajo et al., 2016; Ries et al., 2009). Especially in a system where species and phenotypic diversity is already limited, natural selection simply creates an even more limited, and therefore less resilient, system. Other environmental stressors represent an additional challenge to understanding this resilience: at this stage, the impacts of acidification on ecosystems are too small to distinguish from inter-annual variations and other forms of climate change already linked to major ecosystem perturbations. Rather than indicating overall ecosystem resilience to acidification, initial indications of resilience may instead simply mask acidification impacts, with much more dramatic results likely to emerge as the system passes critical thresholds. For example, while red king crab larvae and juveniles are vulnerable to OA, models project that the impacts on recruitment and population density will be limited for the next 10–20 years and could be masked by the effects of natural variation in temperature or climate patterns before severe impacts of OA rapidly emerge (Punt et al., 2016).

Given the uncertainty about the balance between ecosystem-level vulnerability and resilience, it is imperative to continue ocean research and monitoring and Alaska-specific laboratory acidification studies across multiple scales in order to support commercial industries, coastal communities, and subsistence fisheries in the PAR. As anthropogenic climate change continues to alter the Arctic environment, both vulnerability and resilience of Arctic ecosystems will continue to change. Acidification stress will continue to worsen; even under the most optimistic emissions scenarios for the next several decades (Bopp et al., 2013; Gattuso et al., 2015), the Chukchi and Beaufort seas are projected to experience persistent surface layer undersaturations beginning in the next few decades (2050–2060; Mathis et al., 2015). Even where acidification is not the primary stress on the environment (e.g. Mayor et al., 2015), it does increase the risk of compounding synergistic impacts from other stressors, like warming, hypoxia, and sea-ice losses (e.g. Gruber, 2011; Byrne and Przeslawski, 2013; Todgham and Stillman, 2013; Kroeker et al., 2013). Many studies predict that the future Arctic will be much different than the one we see today (Grebmeier, 2012; Doney et al., 2012; Renaud et al., 2015). Evidence-based decision making in the face of these changes has the potential to build adaptive capacity for human communities (Mathis et al., 2015a; Inuit Circumpolar Council-Alaska (ICCA), 2015; Lam et al., 2016) and prevent potential fishery crashes, like the projected reduction in population and catch of crab in Bristol Bay (Punt et al., 2014). A solid research footing will help make those efforts as successful as possible.

5. Conclusions

The oceans of the PAR have rapidly acidified over the last several decades as a result of the natural vulnerability of high-latitude waters, a variety of natural acidification mechanisms, and intrusion of anthropogenic CO_2. In this study, we synthesized four recent programs in order to investigate the formation and transport of these corrosive water masses. In the Laptev and East Siberian Seas, river discharge and respiration of terrestrial organic matter was observed to create strong Ω_{Ar} undersaturations. Our projections of pre-industrial conditions indicate that these Ω_{Ar} undersaturations likely emerged without anthropogenic influences, although absorption of anthropogenic CO_2 substantially increased the duration, intensity, and extent of this corrosivity. In the Chukchi Sea, present-day Ω_{Ar} undersaturations were found in the slow-moving waters to the north, where accumulation of respiration productions occurring in conjunction with cooling and salinization produced almost uniformly corrosive PWW that ventilates the Pacific halocline layer. However, in shallower areas and in the Alaska Coastal Current, mixing and consistent sea-air exchange prevented strong carbon accumulation and Ω_{Ar} undersaturations. In the Beaufort Sea, wind-driven upwelling of corrosive Pacific halocline water can completely flush the narrow shelf, producing an episodic OA event but also facilitating the return of a substantial amount of carbon from the ocean to the atmosphere. However, combined with other mechanisms of carbon accumulation, air-sea exchange of CO_2 occurring during upwelling events was not sufficient to mitigate Ω_{Ar} undersaturations.

The corrosive waters formed over the shelves in the PAR were shown to penetrate deep into the Canada Basin and all the way into the Canadian Arctic Archipelago – and hence likely into the North Atlantic. While biological impacts from this recent acidification remain unclear, they could have detrimental effects on ecosystems already undergoing substantial environmental pressure from other forms of global climate change. Prey and predators dependent on the slower advective transport pathways between the Pacific and Arctic Oceans and the seasonal ice zone along the northern Chukchi and Beaufort Shelves may be particularly at risk, given the duration and severity of exposure to seasonal undersaturations. In order to support the management and sustainability of the fisheries in the PAR, it will be critical to continue to monitor global emissions and the rate of OA in the Arctic.

Acknowledgements

We sincerely thank our colleagues involved with the four synthesis programs included in this research. Interdisciplinary work in the Arctic is providing the foundation for closer international collaborations and unprecedented new opportunities. We owe a debt of gratitude to the outstanding officers and crew of the research vessels that make this work possible. We also thank our colleagues who contributed time and energy towards data collection, analysis, and programming, especially Carolina Nobre, Natalie Monacci, Kristen Shake, and Leif Anderson. We are also grateful for our colleagues in the Arctic research community and the Synthesis of Arctic Research (SOAR) program, whose enthusiasm and expertise benefited the preparation, focus, and connections in this manuscript and special issue. SOAR is funded primarily by

the US Department of the Interior, Bureau of Ocean and Energy Management, Environmental Studies Program through Interagency Agreement No. M11PG00034 with the US Department of Commerce (DOC), National Oceanic and Atmospheric Administration (NOAA), Office of Oceanic and Atmospheric Research (OAR), Pacific Marine Environmental Laboratory (PMEL). This manuscript is PMEL contribution No. 4584. This synthesis was also supported by the National Science Foundation Grant PLR-1303617.

Appendix A. Supplementary material

Supplementary data associated with this article can be found in the online version at doi:10.1016/j.dsr2.2018.05.020.

References

AMAP, 1998. AMAP Assessment Report: Arctic Pollution Issues. Arctic Monitoring and Assessment Programme (AMAP), Oslo, Norway, pp. 859.

Almén, A.-K., Vehmaa, A., Brutemark, A., Engström-Öst, J., 2014. Coping with climate change? Copepods experience drastic variations in their physiochemical environment on a diurnal basis. J. Exp. Mar. Biol. Ecol. 460, 120–128. https://doi.org/10.1016/j.jembe.2014.07.001.

Anderson, L.G., Jutterström, S., Hjalmarsson, S., Wåhlström, I., Semiletov, I.P., 2009. Outgassing of CO_2 from Siberian Shelf seas by terrestrial organic matter decomposition. Geophys. Res. Lett. 36, L20601. https://doi.org/10.1029/2009GL040046.

Anderson, L.G., Tanhua, T., Björk, G., Hjalmarsson, S., Jones, E.P., Jutterström, S., Rudels, B., Swift, J.H., Wåhlström, I., 2010. Arctic ocean shelf-basin interaction: an active continental shelf CO_2 pump and its impact on the degree of calcium carbonate solubility. Deep-Sea Res. I 57, 869–879. https://doi.org/10.1016/j.dsr.2010.03.012.

Anderson, L.G., Andersson, P.S., Björk, G., Jones, E.P., Jutterstrom, S., Wåhlström, I., 2013. Source and formation of the upper halocline of the Arctic Ocean. J. Geophys. Res. Oceans 118 (1), 410–421. https://doi.org/10.1029/2012JC008291.

Andersson, A.J., Gledhill, D., 2013. Ocean acidification and coral reefs: effects on breakdown, dissolution, and net ecosystem calcification. Annu. Rev. Mar. Sci. 5, 321–348. https://doi.org/10.1146/annurev-marine-121211-172241.

Arrigo, K.R., van Dijken, G.L., 2015. Continued increases in Arctic Ocean primary production. Prog. Oceanogr. 136, 60–70. https://doi.org/10.1016/j.pocean.2015.05.002.

Azetsu-Scott, K., Clarke, A., Falkner, K., Hamilton, J., Jones, E.P., Lee, C., Petrie, B., Prinsenberg, S., Starr, M., Yeats, P., 2010. Calcium carbon saturation states in the waters of the Canadian Arctic Archipelago and the Labrador Sea. J. Gephys. Res. Oceans 115 (C11). https://doi.org/10.1029/2009JC005917.

Bates, N.R., 2015. Assessing ocean acidification variability in the Pacific-Arctic Region as part of the Russian-American Long-term Census of the Arctic. Oceanography 28 (3), 36–45. https://doi.org/10.5670/oceanog.2015.56.

Bates, N.R., Mathis, J.T., 2009a. The Arctic Ocean marine carbon cycle: evaluation of air-sea CO_2 exchanges, ocean acidification impacts, and potential feedbacks. Biogeoscience 6, 2433–2459. https://doi.org/10.5194/bg-6-2433-2009.

Bates, N.R., Mathis, J.T., Cooper, L.W., 2009b. Ocean acidification and biologically induced seasonality of carbonate mineral saturation states in the western Arctic Ocean. J. Geophys. Res. 114, C11007. https://doi.org/10.1029/2008JC004862.

Bates, N.R., Cai, W.-J., Mathis, J.T., 2011. The ocean carbon cycle in the Western Arctic Ocean: distributions and air-sea fluxes of carbon dioxide. Oceanography 24 (3), 186–201. https://doi.org/10.5670/oceanog.2011.71.

Bates, N.R., Orchowska, M.I., Garley, R., Mathis, J.T., 2013. Summertime calcium carbonate undersaturation in shelf waters of the western Arctic Ocean – how biological processes exacerbate the impact of ocean acidification. Biogeoscience 10, 5281–5309. https://doi.org/10.5194/bg-10-5281-2013.

Bates, N.R., Astor, Y.M., Church, M.J., Currie, K., Dore, J.E., González-Dávila, M., et al., 2014a. A time-series view of changing ocean chemistry due to ocean uptake of anthropogenic CO_2 and ocean acidification. Oceanography 27 (1), 126–141. https://doi.org/10.5670/oceanog.2014.16.

Bates, N.R., Garley, R., Frey, K.E., Shake, K.L., Mathis, J.T., 2014b. Sea-ice melt CO_2-carbonate chemistry in the western Arctic Ocean: meltwater contributions to air-sea CO_2 gas exchange, mixed-layer properties and rates of net community production under sea ice. Biogeoscience 11, 6769–6789. https://doi.org/10.5194/bgd-11-1097-2014.

Bluhm, B.A., Walker, D.A., Walsh, J.H., Carmack, E.C., Frey, K., Meier, M.N., Moore, S.E., Parmentier, F.-J.W., Post, E., Romanovsky, V.E., Simpson, W.M., 2014. Implications of Arctic sea-ice decline for the earth system. Ann. Rev. Environ. Res. 39, 12.1–12.33. https://doi.org/10.1146/annurev-environ-122012-094357.

Bond, N., Stabeno, P.J., Napp, J., 2018. Flow patterns in the Chukchi Sea based on an Ocean Reanalysis, June through October 1979–2014. Deep-Sea Res. II35–47.

Bopp, L., Resplandy, L., Orr, J.C., Doney, S.C., Dunne, J.P., Gehlen, M., Halloran, P., Heinze, C., Ilyina, T., Seferian, R., et al., 2013. Multiple stressors of ocean ecosystems in the 21st century: projections with CMIP5 models. Biogeoscience 10 (6), 6225–6245. https://doi.org/10.5194/bg-10-6225-2013.

Boyd, P.W., 2011. Beyond ocean acidification. Nat. Geosci. 4, 273–274. https://doi.org/10.1038/ngeo1150.

Buesseler, K.O., 1998. The decoupling of production and particulate export in the surface ocean. Glob. Biogchem. Cycl. 12 (2), 297–310. https://doi.org/10.1029/97GB03366.

Butterworth, B.J., Miller, S.D., 2016. Air-sea exchange of carbon dioxide in the Southern Ocean and Antarctic marginal ice zone. Geophys. Res. Lett. 43 (13), 7223–7230. https://doi.org/10.1002/2016GL069581.

Byrne, M., Przeslawski, R., 2013. Multistressor impacts of warming and acidification of the ocean on marine invertebrates' life histories. Integr. Comp. Biol. 53 (4), 582–596. https://doi.org/10.1093/icb/ict049.

Caldeira, K., Wickett, M.E., 2003. Anthropogenic carbon and pH. Nature 425 (6956), 365. https://doi.org/10.1038/425365a.

Carmack, E., Wassman, P., 2006. Food webs and physical-biological coupling on pan-Arctic shelves: unifying concepts and comprehensive perspectives. Prog. Oceanogr. 71, 446–477. https://doi.org/10.1016/j.pocean.2006.10.004.

Charkin, A.N., Dudarev, O.V., Semiletov, I.P., Kruhmalev, A.V., Vonk, J.E., Sanchéz-García, L., Karlsson, E., Gustafsson, Ö., 2011. Seasonal and interannual variability of sedimentation and organic matter distribution in the Buor-Khaya Gulf: the primary recipient of input from Lena River and coastal erosion in the southeast Laptev Sea. Biogeoscience 8, 2581–2594. https://doi.org/10.5194/bg-8-2581-2011.

Chen, C.-T.A., 1993. The oceanic anthropogenic CO_2 sink. Chemosphere 27 (6), 1041–1064. https://doi.org/10.1016/0045-6535(93)90067-F.

Citta, J.J., Okkonen, S.R., Quakenbush, L.T., Maslowski, W., Osinksi, R., George, J.C., Small, R.J., Brower Jr., H., Heide-Jørgensen, M.P., Harwood, L.A., 2018. Oceanographic characteristics associated with autumn movements of bowhead whales in the Chukchi Sea. Deep-Sea Res. II 121–131. https://doi.org/10.1016/j.dsr2.2017.03.009.

Citta, J.J., Quakenbush, L.T., Okkonen, S.R., Druckenmiller, M.L., Maslowski, W., Clement-Kinney, J., George, J.C., Brower, H., Small, R.J., Ashjian, C.J., Harwood, L.A., Heide-Jørgensen, M.P., 2015. Ecological characteristics of core-use areas used by Bering-Chukchi-Beaufort (BCB) bowhead whales, 2006–2012. Prog. Oceanogr. 136, 201–222. https://doi.org/10.1016/j.pocean.2014.08.012.

Coachman, L.K., 1986. Circulation, water masses, and fluxes on the southeastern Bering Sea shelf. Cont. Shelf Res. 5, 23–108. https://doi.org/10.1016/0278-4343(86)90011-7.

Codispoti, L.A., Flagg, C., Kelly, V., Swift, J.H., 2005. Hydrographic conditions during the 2002 SBI process experiments. Deep Sea Res. II 52 (24–26), 3199–3226. https://doi.org/10.1016/j.dsr2.2005.10.007.

Codispoti, L.A., Kelly, V., Thessen, A., Matrai, P., Suttles, S., Hill, V., Steele, M., Light, B., 2013. Synthesis of primary production in the Arctic Ocean: iii. Nitrate and phosphate based estimates of net community production. Oceanography 110, 126–150. https://doi.org/10.1016/j.pocean.2012.11.006.

Cooper, L.W., McClelland, J.W., Holmes, R.M., Raymond, P.A., Gibson, J.J., Guay, C.K., Peterson, B.J., 2008. Flow-weighted values of runoff tracers ($\delta^{18}O$, DOC, Ba, alkalinity) from the six largest Arctic rivers. Geophys. Res. Lett. 35 (18), L18606. https://doi.org/10.1029/2008GL035007.

Cooper, H.L., Potts, D.C., Paytan, A., 2016. Effects of elevated pCO_2 on the survival, growth, and moulting of the Pacific krill species, *Euphausia pacifica*. ICES J. Mar. Sci. https://doi.org/10.1093/icesjms/fsw021.

Corlett, W.B., Pickart, R.S., 2017. The Chukchi slope current. Prog. Oceanogr. 153, 50–65. https://doi.org/10.1016/j.pocean.2017.04.005.

Cripps, G., Lindeque, P., Flynn, K.J., 2014. Have we been underestimating the effects of ocean acidification in zooplankton? Glob. Biol. 20 (11), 3377–3385. https://doi.org/10.1111/gcb.12582.

Cross, J.N., Mathis, J.T., Bates, N.R., 2012. Hydrographic controls on net community production and total organic carbon distributions in the eastern Bering Sea. Deep-Sea Res. II 65–70, 98–109. https://doi.org/10.1016/j.dsr2.2012.02.003.

Cross, J.N., Mathis, J.T., Bates, N.R., Byrne, R.H., 2013. Conservative and non-conservative variations of total alkalinity on the southeastern Bering Sea shelf. Mar. Chem. 154, 100–112. https://doi.org/10.1016/j.marchem.2013.05.012.

Cross, J.N., Mathis, J.T., Frey, K.E., Cosca, C.E., Danielson, S.L., Bates, N.R., Feely, R.A., Takahashi, T., Evans, W., 2014. Annual sea-air CO_2 fluxes in the Bering Sea: insights from new autumn and winter observations of a seasonally ice-covered continental shelf. J. Geophys. Res., Oceans 119, 6693–6708. https://doi.org/10.1002/2013JC009579.

Dahlke, F.T., Leo, E., Mark, F.C., Pörtner, H.-O., Bickmeyer, U., Fickenhaus, S., Storch, D., 2016. Effects of ocean acidification increase embryonic sensitivity to thermal extremes in Atlantic cod *Gadus morhua*. .Glob. Biol. https://doi.org/10.1111/gcb.13527.

De Wit, P., Dupont, S., Thor, P., 2015. Selection on oxidative phosphorylation and ribosomal structure as a multigenerational response to ocean acidification in the common copepod *Pseudocalanus acuspes*. Evol. Appl. 9, 1112–1123. https://doi.org/10.1111/eva.12335.

Dickson, A.G., Sabine, C.L., Christian, J.R. (Eds.), 2007. Guide to Best Practices for Ocean CO_2 Measurements 3. PICES Special Publication, pp. 191.

Dickson, A.G., 2010. Standards for ocean measurements. Oceanography 23 (3), 34–47. https://doi.org/10.5670/oceanog.2010.22.

Doney, S.C., Fabry, V.J., Feely, R.A., Kleypas, J.A., 2009. Ocean acidification: the other CO_2 problem. Annu. Rev. Mar. Sci. 1, 169–192. https://doi.org/10.1146/annurev.marine.010908.163834.

Doney, S.C., Ruckelshaus, M., Duffy, J.E., Barry, J.P., Chan, F., English, C.A., Galindo, H., Grebmeier, J.M., Hollowed, A.B., Knowlton, N., Polovina, J., Rabalais, N.N., Sydeman, W.J., Talley, L.D., 2012. Climate change impacts on marine ecosystems. Ann. Rev. Mar. Sci. 4, 11–37. https://doi.org/10.1146/annurev-marine-041911-111611.

Evans, W., Cross, J.N., Mathis, J.T., 2014. Calcium carbonate corrosivity in an Alaskan inland sea. Biogeoscience 11, 365–379. https://doi.org/10.5194/bg-11-365-2014.

Evans, W., Mathis, J.T., Cross, J.N., Bates, N.R., Frey, K.E., Else, B.G.T., Papakyriakou, T.N., DeGrandpre, M.D., Islam, F., Cai, W.-J., Chen, B., Yamamoto-Kawai, M., Carmack, E., Williams, W.J., Takahashi, T., 2015. Sea-air CO_2 exchange in the

western Arctic coastal ocean. Glob. Biogeochem. Cycles 29 (8), 1190–1209. https://doi.org/10.1002/2015GB005153.
Fabry, V.J., Seibel, B.A., Feely, R.A., Orr, J.C., 2008. Impacts of ocean acidification of marine fauna and ecosystem processes. ICES J. Mar. Sci. 65 (3), 414–432. https://doi.org/10.1093/icesjms/fsn048.
Fabry, V.J., McClintock, J.B., Mathis, J.T., Grebmeier, J.M., 2009. Ocean acidification at high latitudes: the bellwether. Oceanography 22 (4), 160–171. https://doi.org/10.5670/oceanog.2009.105.
Feely, R.A., Doney, S.C., Cooley, S.R., 2009. Ocean acidification: present conditions and future changes in a high-CO_2 world. Oceaongraphy 22 (4), 36–47. https://doi.org/10.5670/oceanog.2009.95.
Ferrari, M.C.O., McCormick, M.I., Munday, P.L., Meekan, M.G., Dixson, D.L., Lonnstedt, Ö., Chivers, D.P., 2011. Putting prey and predator into the CO_2 equation – qualitative and quantitative effects of ocean acidification on predator-prey interactions. Ecol. Lett. 14 (11), 1143–1148. https://doi.org/10.1111/j.1461-0248.2011.01683.x.
Fortier, M., Fortier, L., Michel, C., Legendre, L., 2002. Climatic and biological forcing of the vertical flux of biogenic particles under seasonal Arctic sea ice. Mar. Ecol. Prog. Ser. 225, 1–16. https://doi.org/10.3354/meps225001.
Frommel, A.Y., Maneja, R., Lowe, D., Malzahn, A.M., Geffen, A.J., Folvord, A., Piatkowski, U., Reusch, T.B.H., Clemmesen, C., 2012. Severe tissue damage in Atlantic cod under increasing ocean acidification. Nat. Clim. Change 2, 42–46. https://doi.org/10.1038/nclimate1324.
Gattuso, J.P., Magnan, A., Billé, R., Cheung, W.W.L., Howes, E.L., Joos, F., et al., 2015. Contrasting futures for ocean and society from different anthropogenic CO_2 emissions scenarios. Science 349 (6243), aac4722. https://doi.org/10.1126/science.aac4722.
Gazeau, F., Quiblier, C., Jansen, J.M., Gattuso, J.-P., Middelburg, J.J., Heip, C.H.R., 2007. Impact of elevated CO_2 on shellfish calcification. Geophys. Res. Lett. 34 (7), L07603. https://doi.org/10.1029/2006GL028554.
Gazeau, F., Parker, L.M., Comeau, S., Gattuso, J.-P., O'Connor, W.A., Martin, S., Pörtner, H.-O., Ross, P.M., 2013. Impacts of ocean acidification on marine shelled molluscs. Mar. Biol. 160 (8), 2207–2245. https://doi.org/10.1007/s00227-013-2219-3.
Goethel, C.L., Grebmeier, J.M., Cooper, L.W., Miller, T.J., 2017. Implications of ocean acidification in the Pacific Arctic: experimental responses of three Arctic bivalves to decreased pH and food availability. Deep-Sea Res. II 144, 112–124. https://doi.org/10.1016/j.dsr2.2017.08.013.
Gong, D., Pickart, R.S., 2015. Summertime circulation in the eastern Chukchi Sea. Deep-Sea Res. II 118A, 18–31. https://doi.org/10.1016/j.dsr2.2015.02.006.
Grebmeier, J.M., 2012. Shifting patterns of life in the Pacific Arctic and sub-Arctic Seas. Ann. Rev. Mar. Sci. 4, 63–78. https://doi.org/10.1146/annurev-marine-120710-100926.
Grebmeier, J.M., Maslowski, W. (Eds.), 2014. The Pacific Arctic Region. Springer Science +Business Media, Dordecht. https://doi.org/10.1007/978-94-017-8863-2.
Grebmeier, J.M., Overland, J.E., Moore, S.E., Farley, E.V., Carmack, E.C., Cooper, L.W., Frey, K.E., Helle, J.H., McLaughlin, F.A., McNutt, S.L., 2006. A major ecosystem shift in the northern Bering Sea. Science 311 (5766), 1461–1464. https://doi.org/10.1126/science.1121365.
Gruber, N., 2011. Warming up, turning sour, losing breath: ocean biogeochemistry under global change. Philos. Trans. R. Soc. A 369 (1943), 1980–1996. https://doi.org/10.1098/rsta.2011.0003.
Gustafsson, E., Humborg, C., Bjork, G., Stranne, C., Anderson, L.G., Geibel, C., Morth, C.-M., Sundborn, M., Semiletov, I.P., Thornton, B.F., Gustafsson, B.G., 2017. Carbon cycling on the East Siberian Arctic Shelf – a change in air-sea CO_2 flux induced by mineralization of terrestrial organic carbon. Biogeosci. Disc. https://doi.org/10.5194/bg-2017-115.
Haeckey, P., Jonsson, S., Andersson, A., 1998. Influence of sea ice on the composition of the spring phytoplankton bloom in the northern Baltic Sea. Pol. Biol. 20, 1–8. https://doi.org/10.1007/s003000050270.
Haeckey, P., Andersson, A., 1999. Primary and bacterial production in sea ice in the northern Baltic Sea. Aquat. Microb. Ecol. 20, 107–118. https://doi.org/10.3354/ame020107.
Hall-Spencer, J.M., Rodolfo-Metalpa, R., Martin, S., Ransome, E., Fine, M., Turner, S.M., Rowley, S.J., Tedesco, D., Buia, M.-C., 2008. Volcanic carbon dioxide vents show ecosystem effects of ocean acidification. Nature 454, 96–99. https://doi.org/10.1038/nature07051.
Hansell, D.A., Whitledge, T.E., Goering, J.J., 1993. Patterns of nitrate utilization and new production over the Bering-Chukchi shelf. Cont. Shelf. Res. 13 (5–6), 601–627. https://doi.org/10.1016/0278-4343(93)90096-G.
Hill, V., Ardyna, M., Lee, S.H., Varela, D.E., 2018. Decadal trends in phytoplankton production in the Pacific Arctic Region from 1950 to 2012. Deep-Sea Res. II. 82–94. https://doi.org/10.1016/j.dsr2.2016.12.015.
Hill, V., Cota, G., 2005. Spatial patterns of primary production on the shelf, slope, and basin of the Western Arctic in 2002. Deep Sea Res. II 52 (24–26), 3344–3354. https://doi.org/10.1016/j.dsr2.2005.10.001.
Hilton, R.G., Galy, V., Gaillardet, J., Dellinger, M., Byrant, C., O'Regan, M., Grocke, D.R., Coxall, H., Bouchez, J., Calmels, D., 2015. Erosion of organic carbon in the Arctic as a geologic carbon dioxide sink. Nature 524 (7563), 84–97 (doi: 1038/nature14653).
Hofmann, G.E., Barry, J.P., Edmunds, P.J., Gates, R.D., Hutchins, D.A., Klinger, T., Sewell, M.A., 2010. The effect of ocean acidification on calcifying organisms in marine ecosystems: an organism – to – ecosystem perspective. Annu. Rev. Ecol. Evol. Syst. 41, 127–147. https://doi.org/10.1146/annurev.ecolsys.110308.120227.
Hollowed, A.B., Barange, M., Beamish, R.J., Brander, K., Cochrane, K., Drinkwater, K., Foreman, M.G.G., Hare, J.A., Holt, J., Ito, S.-I., et al., 2013. Projected impacts of climate change on marine fish and fisheries (doi.org/). ICES J. Mar. Sci. 70 (5), 1023–1037. https://doi.org/10.1093/icesjms/fst081.
Hönisch, B., Ridgwell, A., Schmidt, D.N., Thomas, E., Gibbs, S., Slujs, A., Zeebe, R., Kump, L., et al., 2012. The geological record of ocean acidification. Science 335 (6072), 1058–1063. https://doi.org/10.1126/science.1208277.
Hydes, D.J., Loucaides, S., Tyrrell, T., 2010. Report on a desk study to identify likely sources of error in the measurements of carbonate system parameters and related calculations, particularly with respect to coastal waters and ocean acidification experiments. Research & Consultancy Report 83, National Oceanography Centre, Southampton. Available at http://nora.nerc.ac.uk/id/eprint/270235/.
Inuit Circumpolar Council-Alaska (ICCA), 2015. Alaskan Inuit Food Security Conceptual Framework: How to Assess the Arctic From an Inuit Perspective: Summary Report and Recommendations Report. ICCA, Anchorage, AK.
Itoh, M., Shimada, K., Kamoshida, T., McLaughlin, F., Carmack, E., Nishino, S., 2012. Interannual variability of Pacific Winter Water inflow through Barrow Canyon from 2000 to 2006. J. Oceanogr. 68, 575–592. https://doi.org/10.1007/s10872-012-0120-1.
Jay, C.V., Fischbach, A.S., Kochnev, A.A., 2012. Walrus areas of use in the Chukchi Sea during sparse sea-ice cover. Mar. Ecol. Prog. Ser. 468, 1–13. https://doi.org/10.3354/meps10057.
Joint, I., Doney, S.C., Karl, D.M., 2011. Will ocean acidification affect marine microbes? ISME J. 5, 1–7. https://doi.org/10.1038/ismej.2010.79.
Kachel, N.B., Hunt Jr., G.L., Salo, S.A., Schumacher, J.D., Stabeno, P.J., Whitledge, T.E., 2002. Deep Sea Res. II 49 (26), 5889–5909. https://doi.org/10.1016/S0967-0645(02)00324-7.
Kawaguchi, S., Ishida, A., King, R., Raymond, B., Waller, N., Constable, A., Nicol, S., Wakita, M., Ishimatsu, A., 2013. Risk maps for Antarctic krill under projected Southern Ocean acidification. Nat. Clim. Change 3, 843–847. https://doi.org/10.1038/NCLIMATE1937.
Kelly, M.W., Hofmann, G.E., 2012. Adaptation and the physiology of ocean acidification. Funct. Ecol. 27 (4), 980–990. https://doi.org/10.1111/j.1365-2435.2012.02061.x.
Kroeker, K.J., Kordas, R.L., Crim, R.N., Singh, G.G., 2010. Meta-analysis reveals negative yet variable effects of ocean acidification on marine organisms. Ecol. Lett. 13 (11), 1419–1434. https://doi.org/10.1111/j.1461-0248.2010.01518.x.
Kroeker, K.J., Kordas, R.L., Crim, R., Hendriks, I.E., Singh, G.S., Duarte, C.M., Gattuso, J.-P., 2013. Impacts of ocean acidification on marine organisms: quantifying sensitivities and interaction with warming. Glob. Change Biol. 19 (6), 1884–1896. https://doi.org/10.1111/gcb.12179.
Kuletz, K.J., Ferguson, M.C., Hurley, B., Gall, A.E., Labunski, E.A., Morgan, T.C., 2015. Seasonal spatial patterns in seabird and marine mammal distribution in the eastern Chukchi and western Beaufort sea: identifying biologically important pelagic areas. Prog. Oceanogr. 136, 175–200. https://doi.org/10.1016/j.pocean.2015.05.012.
Kulkarni, T., Watkins, J.M., Nickels, S., Lemmen, D.S., 2012. Canadian International Polar Year (2007–2008). Clim. Change 115 (1), 1–11. https://doi.org/10.1007/s10584-012-0583-5.
Kunz, K.L., Frickenhaus, S., Hardenberg, S., Johansen, T., Leo, E., Portner, H.-O., Schmidt, M., Windisch, S., Knust, R., Mark, F.C., 2016. New encounters in Arctic waters: a comparison of metabolism and performance of polar cod (*Boreogadus saida)* and Atlantic cod (*Gadus morhua)* under ocean acidification and warming. Polar Biol. 39 (6), 1137–1153. https://doi.org/10.1007/s00300-016-1932-z.
Kurihara, H., 2008. Effects of CO_2-driven ocean acidification on the early developmental stages of invertebrates. Mar. Ecol. Prog. Ser. 373, 275–284. https://doi.org/10.3354/meps07802.
Lam, V.W.Y., Cheung, W.W.L., Sumaila, U.R., 2016. Marine capture fisheries in the Arctic: winners or losers under climate change and ocean acidification? Fish. Fish. 17, 335–357. https://doi.org/10.1111/faf.12106.
Laruelle, G.G., Lauerwald, R., Pfiel, B., Regnier, P., 2014. Regionalized global budget of the CO_2 exchange at the air-water interface in continental shelf seas. Glob. Biogeochem. Cy 28 (11), 1199–1214. https://doi.org/10.1002/2014GB004832.
Le Quéré, C., Moriarty, R., Andrew, R.M., Peters, G.P., Friedlingstein, P., Jones, S.D., et al., 2015. Global carbon budget 2014. Earth Sci. Syst. Data 7, 47–85. https://doi.org/10.5194/essd-7-47-2015.
Leu, E., Søreide, J.E., Hessen, D.O., Falk-Peterson, S., Berge, J., 2011. Consequences of changing sea-ice cover for primary and secondary producers in the European Arctic shelf seas: timing, quantity, and quality. Prog. Oceanogr. 90 (1–4), 18–32. https://doi.org/10.1016/j.pocean.2011.02.004.
Lin, P., Pickart, R.S., Stafford, K.M., Moore, G.W.K., Torres, D.J., Bahr, F., Hu, J., 2016. Seasonal variations of the Beaufort shelfbreak jet and its relationship to Arctic cetacean occurrence. J. Geophys. Res. 121 (12), 8434–8454. https://doi.org/10.1002/2016JC011890.
Llinás, L., Pickart, R.S., Mathis, J.T., Smith, S.L., 2009. Zooplankton inside an Arctic Ocean cold-core eddy: probable origin and fate. Deep Sea Res. II 56 (17), 1290–1304. https://doi.org/10.1016/j.dsr2.2008.10.020.
Logerwell, E., Rand, K., Danielson, S., Sousa, L., 2018. Environmental drivers of benthic fish distribution in and around Barrow Canyon in the northeastern Chukchi Sea and western Beaufort Sea. Deep-Sea Res., II. 170–181. https://doi.org/10.1016/j.dsr2.2017.04.012.
Long, W.C., Swiney, K.M., Harris, C., Page, H.N., Foy, R.J., 2013a. Effects of ocean acidification on juvenile Red King crab (Paralithodes camtschaticus) and Tanner crab (Chinoecetes bairdi) growth, condition, calcification, and survival. PLOS One 8 (4), e60959. https://doi.org/10.1371/journal.pone.0060959.
Long, W.C., Swiney, K.M., Foy, R.J., 2013b. Effects of ocean acidification on the embryos and larvae of red king crab, *Paralithodes camtschaticus*. Mar. Pol. Bull. 69, 38–47. https://doi.org/10.1016/j.marpolbul.2013.01.011.
Lowry, K.E., Pickart, R.S., Mills, M.M., Brown, Z.W., van Dijken, G.L., Bates, N.R., Arrigo, K.R., 2015. The influence of winter water on phytoplankton blooms in the Chukchi Sea. Deep Sea Res. II 118A, 53–72. https://doi.org/10.1016/j.dsr2.2015.06.006.
Mathis, J.T., Questel, J.M., 2013. Assessing seasonal changes in carbonate parameters across small spatial gradients in the northeastern Chukchi Sea. Cont. Shelf Res. 67, 42–51. https://doi.org/10.1016/j.csr.2013.04.041.

Mathis, J.T., Hansell, D.A., Kadko, D., Bates, N.R., Cooper, L.W., 2007. Determining net dissolved organic carbon production in the hydrographically complex western Arctic Ocean. Limnol. Oceanogr. 52 (5), 1789–1799. https://doi.org/10.4319/lo.2007.52.5.1789.

Mathis, J.T., Cross, J.N., Bates, N.R., 2011a. The role of ocean acidification in systemic carbonate mineral suppression in the Bering Sea. Geohpys. Res. Lett. 38, L19602. https://doi.org/10.1029/2011GL048884.

Mathis, J.T., Cross, J.N., Bates, N.R., 2011b. Coupling primary production and terrestrial runoff to ocean acidification and carbonate mineral suppression in the eastern Bering Sea. J. Geophys. Res. 116, C02030. https://doi.org/10.1029/2010JC006453.

Mathis, J.T., Pickart, R.S., Byrne, R.H., McNeil, C.L., Moore, G.W.K., Juranek, L.W., Liu, X., Ma, J., Easley, R.A., Elliot, M.M., Cross, J.N., Reisdorph, S.C., Bahr, F., Morison, J., Lichendorf, T., Feely, R.A., 2012. Storm-induced upwelling of high pCO_2 waters onto the continental shelf of the western Arctic Ocean and implications for carbonate mineral saturation states. Geophys. Res. Lett. 39, L07606. https://doi.org/10.1029/2012GL051574.

Mathis, J.T., Cross, J.N., Monacci, N., Feely, R.A., Stabeno, P., 2013. Evidence of prolonged aragonite undersaturations in the bottom waters of the southern Bering Sea shelf from autonomous sensors. Deep-Sea Res. II 109, 125–133. https://doi.org/10.1016/j.dsr2.2013.07.019.

Mathis, J.T., Cooley, S.R., Lucey, N., Colt, S., Ekstrom, J., Hurst, T., Hauri, C., Evans, W., Cross, J.N., Feely, R.A., 2015a. Ocean acidification risk assessment for Alaska's fishery sector. Prog. Oceanogr. 136, 71–91. https://doi.org/10.1016/j.pocean.2014.07.001.

Mathis, J.T., Cross, J.N., Doney, S.C., 2015b. Ocean acidification in the surface waters of the Pacific-Arctic boundary regions. Oceanography 28 (2), 122–135. https://doi.org/10.5670/oceanog.2015.36.

Mayor, D.J., Sommer, U., Cook, K.B., Viant, M.R., 2015. The metabolic responses of marine copepods to environmental warming and ocean acidification in the absence of food. Sci. Rep. 5, 13690. https://doi.org/10.1038/srep13690.

McBride, M.M., Dalpadado, P., Drinkwater, K.F., Godo, O.R., Hobday, A.J., Hollowed, A.B., et al., 2014. Krill, climate, and contrasting future scenarios for Arctic and Antarctic fisheries. ICES J. Mar. Sci. 71 (7), 1934–1955. https://doi.org/10.1093/icesjms/fsu002.

McLaskey, A.K., Keister, J., McElhaney, P., Olson, M.B., Busch, D.S., Maher, M., Winans, A.K., 2016. 555, 65-78, doi: 10.3354/meps11839.

Millero, F.J., Graham, T.B., Huang, F., Bustos-Serrano, H., Pierrot, D., 2006. Dissociation constants of carbonic acid in seawater as a function of salinity and temperature. Mar. Chem. 100, 80–94. https://doi.org/10.1016/j.marchem.2005.12.001.

Moore, S.E., Stabeno, P.J., Grebmeier, J.M., Okkonen, S.R., 2018. The Arctic Marine Pulses Model: linking annual oceanographic processes to contiguous ecological domains in the Pacific Arctic. Deep-Sea Res. II. 8–21. https://doi.org/10.1016/j.dsr2.2016.10.011.

Moore, S.E., Gulland, F.M.D., 2014. Linking marine mammal and ocean health in the 'New Normal' arctic. Ocean Coast. Manag. 102 (A), 55–57. https://doi.org/10.1016/j.ocecoaman.2014.08.011.

Moore, S.E., Stabeno, P.J., 2015. Synthesis of Arctic Research (SOAR) In marine ecosystems of the Pacific Arctic. Prog. Ocean. 136, 1–11. https://doi.org/10.1016/j.pocean.2015.05.017.

Moore, S.E., Logerwell, E., Eisner, E., Farley Jr., E.V., Harwood, L.A., Kuletz, K., Lovvorn, J., Murphy, J.R., Quakenbush, L.T., 2014. Marine fishes, birds, and mammals as sentinels of ecosystem variability and reorganization in the Pacific Arctic Region (2014) In: Grebmeier, J.M., Maslowski, W. (Eds.), The Pacific Arctic Region. Springer Science + Business Media, Dordecht, pp. 337–392. https://doi.org/10.1007/978-94-017-8863-2.

Moran, S.B., Kelly, R.P., Hagstrom, K., Smith, J.N., Grebmeier, J.M., Cooper, L.W., Cota, G.F., Walh, J.J., Bates, N.R., Hansell, D.A., Maslowski, W., Nelson, R.P., Mulsow, S., 2005. Seasonal changes in POC export flux in the Chukchi Sea and implications for water column-benthic coupling in Arctic shelves. Deep Sea Res. II 52 (24–26), 3427–3451. https://doi.org/10.1016/j.dsr2.2005.09.011.

Nikolopoulos, A., Pickart, R.S., Fratantoni, P.S., Shimada, K., Torres, D.J., Jones, E.P., 2009. The western Arctic boundary current at 152°W: structure, variability, and transport. Deep-Sea Res. II 56, 1164–1181. https://doi.org/10.1016/j.dsr2.2008.10.014.

Okkonen, S.R., Clarke, J.T., Potter, R.A., 2018. Relationships among high river discharges, upwelling events, and bowhead whale (*Balaena mysticetus*) occurance in the central Alaska Beaufort Sea. Deep-Sea Res. II195–202.

Overland, J.E., Stabeno, P.J., 2004. Is the climate of the Bering Sea warming and affecting the ecosystem? EOS Trans. Am. Geophys. Union 85 (33), 309–316. https://doi.org/10.1029/2004EO330001.

Paquette, R.G., Bourke, R.H., 1974. Observations on the coastal current of Arctic Alaska. J. Mar. Res. 32, 195–207.

Pickart, R.S., Stossmeister, G., 2008. Outflow of water from the Chukchi Sea to the Arctic Ocean. Chin. J. Polar Sci. 19 (2), 135–148.

Pickart, R.S., Weingartner, T.J., Zimmermann, S., Torres, D.J., Pratt, L.J., 2005. Flow of winter-transformed Pacific water into the western Arctic. Deep-Sea Res. II 52, 3175–3198. https://doi.org/10.1016/j.dsr2.2005.10.009.

Pickart, R.S., Moore, G.W.K., Torres, D.J., Fratantoni, P.S., Goldsmith, R.A., Yang, J., 2009. Upwelling on the continental slope of the Alaskan Beaufort Sea: storms, ice, and oceanographic response (C))(A13). J. Geophys. Res. Oceans 114 (C1). https://doi.org/10.1029/2008JC005009.

Pickart, R.S., Pratt, L.J., Torres, D.J., Whitledge, T.E., Proshutinsky, A.Y., Aagaard, K., Agnew, T.A., Moore, G.W.K., Dail, H.J., 2010. Evolution and dynamics of the flow through Herald Canyon in the Western Chukchi Sea. Deep-Sea Res. II 57, 5–26. https://doi.org/10.1016/j.dsr2.2009.08.002.

Pickart, R.S., Schulze, L.M., Moore, G.W.K., Charette, M.A., Arrigo, K.R., van Dijken, G., Danielson, S.L., 2013. Long-term trends of upwelling and impacts on primary productivity in the Alaskan Beaufort Sea. Deep-Sea Res. I 79, 106–121. https://doi.org/10.1016/j.dsr.2013.05.003.

Pickart, R.S., Moore, G.W.K., Mao, C., Bahr, F., Nobre, C., Weingartner, T.J., 2016. Circulation of winter water on the Chukchi Shelf in early summer (in press). Deep-Sea Res. II. https://doi.org/10.1016/j.dsr2.2016.05.001.

Punt, A.E., Poljak, D., Dalton, M.G., Foy, R.J., 2014. Evaluating the impact of ocean acidification on fishery yields and profits: the example of red king crab in Bristol Bay. Ecol. Modell. 2014 (285), 39–53. https://doi.org/10.1016/j.ecolmodel.2014.04.017.

Punt, A.E., Foy, R.J., Dalton, M.G., Long, C., Swiney, K.M., 2016. Effects of long-term exposure to ocean acidification conditions on future southern Tanner crab (*Chionoecetes bairdi*) fisheries management. ICES J. Mar. Sci. 73 (3), 849–864. https://doi.org/10.1093/icesjms/fsv205.

Qi, D., Chen, L., Chen, B., Gao, Z., Zhong, W., Feely, R.A., 2016. Increase in acidifying water in the western Arctic Ocean. Nature Climate Change 7, 195–199. https://doi.org/10.1038/nclimate3228.

Questel, J.M., Clarke, C., Hopcroft, R.R., 2013. Seasonal and interannual variation in the planktonic communities of the northeastern Chukchi Sea during the summer and early fall. Cont. Shelf Res. 67, 23–41. https://doi.org/10.1016/j.csr.2012.11.003.

Ramajo, L., Pérez-León, E., Hendriks, I.E., Marbà, N., Krause-Jensen, D., Sejr, M.K., Blicher, M.E., Lagos, N.A., Olsen, Y.S., Duarte, C.M., 2016. Food supply confers calcifiers resistance to ocean acidification. Sci. Rep. 6, 19374. https://doi.org/10.1038/srep19374.

Reigstad, M., Riser, C.W., Wassman, P., Ratkova, T., 2008. Vertical export of particulate organic carbon: attenuation, composition and loss rates in the northern Barents Sea. Deep-Sea Res. II 55 (20–21), 2308–2319. https://doi.org/10.1016/j.dsr2.2008.05.007.

Renaud, P.E., Sejr, M.K., Bluhm, B.A., Sirenko, B., Ellingsen, I.H., 2015. The future of Arctic benthos: expansion, invasion, and biodiversity. Prog. Oceanogr. 139, 244–257. https://doi.org/10.1016/j.pocean.2015.07.007.

Riebesell, U., Schloss, I., Smetacek, V., 1991. Aggregation of algae released from melting sea ice: implications for seeding and sedimentation. Polar Biol. 11 (4), 239–248. https://doi.org/10.1007/BF00238457.

Ries, J.B., Cohen, A.L., McCorkle, D.C., 2009. Marine calcifiers exhibit mixed responses to CO_2-induced ocean acidification. Geology 37 (12), 1131–1134. https://doi.org/10.1130/G30210A.1.

Robbins, L.L., Hansen, M.E., Kleypas, J.A., Meylan, S.C., 2010. CO2calc- a user-friendly seawater carbon calculator for Windows, Mac OS X, and iOS (iPhone). US Geological Survey Open-File Report, 2010–1280, 17 pp. Available at https://pubs.usgs.gov/of/2010/1280/.

Sabine, C.L., Feely, R.A., Gruber, N., Key, R.M., Lee, K., Bullister, J.L., et al., 2004. The oceanic sink for anthropogenic CO_2. Science 305 (5682), 367–371. https://doi.org/10.1126/science.1097403.

Schulze, L.M., Pickart, R.S., 2012. Seasonal variation of upwelling in the Alaskan Beaufort Sea: impact of sea-ice cover. J. Geophys. Res. Oceans 117, C06022. https://doi.org/10.1029/2012JC007985.

Semiletov, I., Pipko, I., Gustafsson, Ö., Anderson, L.G., Sergienko, V., Pugach, S., Dudarev, O., Charkin, A., Gukov, A., Bröder, L., Andersson, A., Spivak, E., Shakhova, N., 2016. Acidification of East Siberian Arctic Shelf waters through addition of freshwater and terrestrial carbon. Nat. Geosci. 9, 361–365. https://doi.org/10.1038/ngeo2695.

Shadwick, E.H., Thomas, H., Gratton, Y., Leong, D., Moore, S.A., Papakyriakou, T., Prowe, A.E.F., 2011. Export of Pacific carbon through the Arctic Archipelago to the North Atlantic. Cont. Shelf Res. 31, 806–816. https://doi.org/10.1016/j.csr.2011.01.014.

Sigler, M.F., Cross, J.N., Dalton, R.J., Foy, T.P., Hurst, T.P., Long, W.C., Nichols, K., Spies, I., Stones, R.P., 2017. NOAA's Alaska Ocean Acidification Research Plan for FY18-FY20. AFSC Processed Rep. 2017-10, 71 p. Alaska Fish. Sci. Cent., NOAA, Natl. Mar. Fish. Serv., 7600 Sand Point Way NE, Seattle WA 98115. Available at ⟨http://www.afsc.noaa.gov/Publications/ProcRpt/PR2017-10.pdf⟩.

Spall, M.A., 2007. Circulation and water mass transformation in a model of the Chukchi Sea. J. Geophysica Res., Oceans 112https://doi.org/10.1029/2005JC003364. C05025.

Spall, M.A., Pickart, R.S., Fratantoni, P.S., Plueddemann, A.J., 2008a. Western Arctic shelfbreak eddies: formation and transport. J. Phys. Oceangr. 38, 1644–1668. https://doi.org/10.1175/2007JPO3829.1.

Spall, M.A., Pickart, Rs, Fratantoni, P.S., Plueddemann, A.J., 2008b. Western Arctic shelfbreak eddies: formation and transport. J. Phys. Oceanogr. 38, 1644–1668. https://doi.org/10.1175/2007JPO3829.1.

Spall, M.A., Pickart, R.S., Brugler, E.T., Moore, G.W.K., Thomas, L., Arrigo, K.R., 2014. Role of shelfbreak upwelling in the formation of a massive under-ice bloom in the Chukchi Sea. Deep Sea Research Part II: Topical Studies in Oceanography, Volume 105, July 2014, Pages 17-29, doi: 10.1016/j.dsr2.2014.03.017.

Steinacher, M., Frölicher, T.L., Plattner, G.-K., Doney, S.C., 2009. Imminent ocean acidification in the Arctic projected with the NCAR global coupled carbon cycle-climate model. Biogeoscience 6, 515–533. https://doi.org/10.5194/bg-6-515-2009.

Stiasny, M.H., Mittemayer, F.H., Sswat, M., Voos, R., Jutfelt, F., Chierici, M., Puvanendran, V., Mortensen, A., Reusch, T.B.H., Clemmesen, C., 2016. Ocean acidification effects on Atlantic cod larval survival and recruitment to the fished population. PLOS One. https://doi.org/10.1371/journal.pone.0155448.

Talmage, S.C., Gobler, C.J., 2010. Effects of past, present, and future ocean carbon dioxide concentrations on the growth and survival of larval shellfish. Proc. Nat. Acad. Sci. 107 (40), 17246–17251. https://doi.org/10.1073/pnas.0913804107.

Tans, P., Keeling, R., 2016. Mauna Loa CO_2 annual mean data. Earth Science Research Laboratory. ⟨ftp://aftp.cmdl.noaa.gov/products/trends/co2/co2_annmean_mlo.txt⟩. (accessed 3 March 2016).

Thor, P., Dupont, S., 2015. Transgenerational effects alleviate severe fecundity loss during ocean acidification in a ubiquitous planktonic copepod (2015). Glob. Chang. Biol. 21

(6), 2261–2271. https://doi.org/10.1111/gcb.12815.
Thor, P., Oliva, E.O., 2015. Ocean acidification elicits different energetic responses in an Arctic and a boreal population of the copepod *Pseudocalanus acuspes*. Mar. Biol. 162, 799–807. https://doi.org/10.1007/s00227-015-2625-9.
Todgham, A.E., Stillman, J.H., 2013. Physiological responses to shifts in multiple environmental stressors: relevance in a changing world. Integr. Comp. Biol. 53 (4), 539–544. https://doi.org/10.1093/icb/ict086.
Tremblay, C., Runge, J.A., Legendre, L., 1989. Grazing and sedimentation of ice algae during and immediately after a bloom at the ice-water interface. Mar. Ecol. Prog. Ser. 56, 291–300.
Tremblay, J.É., Robert, D., Varela, D.E., Lovejoy, C., Darnis, G., Nelson, R.J., Sastri, A.R., 2012. Current state and trends in Canadian Arctic marine ecosystems: I. Primary Production. Clim. Chang. 115 (1), 161–178. https://doi.org/10.1007/s10584-012-0496-3.
Vihtakari, M., Havenhand, J., Renaud, P.E., Hendriks, I.E., 2016. Variable individual- and population-level responses to ocean acidification. Front. Mar. Sci. 3, 51. https://doi.org/10.3389/fmars.2016.00051.
Wang, M., Yang, Q., Overland, J.E., Stabeno, P.J., 2018. Sea-ice cover timing in the Pacific Arctic: The present and projections to mid-century by selected CMIP5 models. Deep-Sea Res. II. 22–34. https://doi.org/10.1016/j.dsr2.2017.11.017.
Wassmann, P., Duarte, C.M., Agust, S., Sejr, M.K., 2011. Footprints of climate change in the Arctic marine ecosystem. Glob. Chang. Biol. 17, 1235–1249. https://doi.org/10.1111/j.1365-2486.2010.02311.x.
Wassman, P., Kosobokova, K.N., Slagstad, D., Drinkwater, K.E., Hopcroft, R.R., Moore, S.E., Ellingsen, I., Nelson, R.J., Carmack, E., Popova, E., Berge, J., 2015. The contiguous domains of Arctic Ocean advection: trails of life and death. Progr. Oceanogr. 139, 42–65. https://doi.org/10.1016/j.pocean.2015.06.011.
Watanabe, Y.W., Chiba, T., Tanaka, T., 2011. Recent change in the oceanic uptake rate of anthropogenic carbon in the North Pacific subpolar region determined using a carbon-13 time series. J. Geophys. Res. 116, C02006. https://doi.org/10.1029/2010JC006199.
Weingartner, T., Aagaard, K., Woodgate, R., Danielson, S., Sasaki, Y., Cavalieri, D., 2005. Circulation on the north central Chukchi Sea shelf. Deep Sea Res. II 52 (24–26), 3150–3174. https://doi.org/10.1016/j.dsr2.2005.10.015.
Woodgate, R.A., Aagaard, K., Weingartner, T.J., 2005a. Monthly temperature, salinity, and transport variability of the Bering Strait throughflow. Geophys. Res. Lett. 32, L04601. https://doi.org/10.1029/2004GL021880.
Woodgate, R.A., Aagaard, K., Weingartner, T.J., 2005b. A year in the physical oceanography of the Chukchi Sea: moored measurements from autumn 1990–1991 (3116-2149). Deep-Sea Res. II 52. https://doi.org/10.1016/j.dsr2.2005.10.016.
Yamamoto-Kawai, M., McLaughlin, F.A., Carmack, E.C., Nishino, S., Shimada, K., Kurita, N., 2009. Surface freshening of the Canada Basin, 2003–2007: river runoff versus sea-ice meltwater. J. Geophys. Res 114, C00A05. https://doi.org/10.1029/2008JC005000.
Yamamoto-Kawai, M., McLaughlin, F., Carmack, E.C., 2013. Ocean acidification in the three oceans surrounding northern North America. J. Geophys. Res. Oceans 118, 6274–6284. https://doi.org/10.1002/2013JC009157.